Dalton Transactions

ROYAL SOCIETY OF CHEMISTRY

PAPER

View Article Online
View Journal | View Issue

Check for updates

Cite this: *Dalton Trans.*, 2025, **54**, 15780

Mono- and dinuclear β-oxo-δ-diiminate (BODDI) based catalysts for the ring-opening polymerization of L-lactide

Fabian Seifert,[a] Dirk F.-J. Piesik,[b] Flavio L. Portwich,[a] Janine Kowalke,[c] Andreas Seifert,[c] Rukiya Matsidik,[c] Helmar Görls,[a] Michael Sommer, [c] Sjoerd Harder *[b,d] and Robert Kretschmer *[a,c,e]

Received 13th August 2025,
Accepted 30th September 2025

DOI: 10.1039/d5dt01934f

rsc.li/dalton

Polyesters such as polylactic acid belong to the most useful biodegradable polymers being able to substitute polyolefins in many applications. In search for potent catalysts based on bio-compatible and non-critical raw materials bimetallic cooperativity has emerged as a powerful approach, but one that is still in its infancy. Here, we report a comparative study on the catalytic activity of overall 13 mono- and dinuclear β-oxo-δ-diiminate (BODDI) complexes in the ring-opening polymerization (ROP) of L-lactide. Variation of the number of metal atoms, the metal, *i.e.*, Li, Mg, Ca, and Zn, as well as of the secondary ligand crucially impacts on the activity of the catalysts and properties of the formed polymers.

Open Access Article. Published on 09 October 2025. Downloaded on 4/7/2026 7:46:47 PM.
This article is licensed under a Creative Commons Attribution 3.0 Unported Licence.

Introduction

Polylactic acid (PLA) derived from natural renewable resources has emerged as one of the leading commercially available sustainable polymers[1] because it is biodegradable under industrial composting conditions[2] and used in a variety of ways, such as in (bio)medical and packaging applications.[3] The industrial production of PLA is mostly based on the ring-opening polymerization (ROP) of L-lactide (L-LA) catalysed by tin(II) 2-ethyl-hexanoate. However, as harmful catalyst residues in the polymeric material are problematic when it comes to (bio)medical applications, the search for less-toxic and environmentally benign alternatives remains a central research theme.[4] In the last decade, cooperative catalysis[5] has been identified as a promising approach also for the ROP of cyclic esters as the interplay of two active sites often yields higher activities and improved selectivities compared to classical single-site catalysts.[6] However, the landscape of dinuclear catalysts is broad, ranging from intermolecular aggregates to tethered systems in which an intramolecular metal–metal interaction is enabled by a suitable ligand framework.[5] Combining two metals within a single molecule overcomes unfavourable monomer/dimer equilibria and steric information of the ligand are possibly transferred to the related product. Hence, homo- and heterobimetallic complexes of ditopic ligands[7] have become attractive research targets in both ROP and ring-opening copolymerization.[6e–i,8] Although the number of homobimetallic catalysts exceeds the number of heterobimetallic examples, comparative studies in which the metal and the number of metals as well as conceivable co-ligands are systematically altered are very rare. The β-oxo-δ-diamine ligand (BODDI) ligand, Fig. 1,[9] provides a suitable scaffold for related studies: the two binding sites are parallel oriented and allow for the installation of two metal centres in close proximity, while the oxygen bridge enables electronic communication of the two metals. However, while macrocyclic BODDI-derived complexes have been intensely used to mimic active sites of enzymes,[9b] the non-fused BODDI relatives have only been utilized in a few cases.[10] Most remarkable is the work by Tonks and co-workers, in which the catalytic activity of monometallic nickel complexes is compared with the respective Ni–alkali

[a]*Institute of Inorganic and Analytical Chemistry (IAAC), Friedrich Schiller University Jena, Humboldtstraße 8, 07743 Jena, Germany*
[b]*Anorganische Chemie, Universität Duisburg-Essen, Universitätsstrasse 5-7, 45117 Essen, Germany*
[c]*Institute of Chemistry, Chemnitz University of Technology, Straße der Nationen 62, 09111 Chemnitz, Germany. E-mail: robert.kretschmer@chemie.tu-chemnitz.de*
[d]*Inorganic and Organometallic Chemistry, Universität Erlangen-Nürnberg, Egerlandstrasse 1, 91058 Erlangen, Germany. E-mail: sjoerd.harder@fau.de*
[e]*Jena Center for Soft Matter (JCSM), Friedrich Schiller University Jena, Philosophenweg 7, 07743 Jena, Germany*

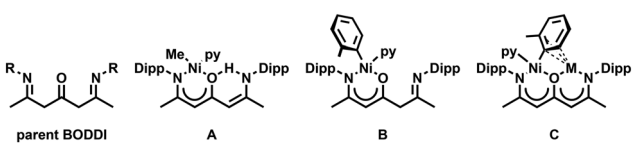

Fig. 1 The parent β-oxo-δ-diamine (BODDI) ligand and mono- (A and B) as well as heterobimetallic (C, M = Li, Na, K) BODDI complexes previously used in ethylene polymerization; Dipp = 2,6-diisopropylphenyl.

This journal is © The Royal Society of Chemistry 2025

Open Access Article. Published on 09 October 2025. Downloaded on 4/7/2026 7:46:47 PM.
This article is licensed under a Creative Commons Attribution 3.0 Unported Licence.

metal heterobimetallic complexes, Fig. 1.[10c] Depending on the co-ligand, they observed two tautomeric forms that show distinctly different activity in ethylene polymerization. In detail, the enamine tautomer Fig. 1A yields low molecular weight polymers while the imine form Fig. 1B as well as the heterobimetallic complexes Fig. 1C give rise to polymers with significantly higher molecular weights. Based on these intriguing findings we set out to synthesize mono- and dinuclear BODDI complexes incorporating calcium, lithium, magnesium, and zinc to explore their catalytic behaviour in ROP of L-lactide. In this work, we describe the synthesis of both, mono- and homobimetallic β-oxo-δ-diiminate (BODDI) complexes. We show that their catalytic activity in the ring-opening polymerization of L-lactide, as well as the properties of the resulting polymers, depend on the metal, the number of metal atoms, and the nature of the second ligand.

Results and discussion

Synthesis and structural characterization of mono- and dinuclear BODDI complexes

Based on the previous work of Coates and co-workers on dinuclear ethyl zinc β-oxo-δ-diiminate complexes,[10a] we have used the protio-ligand **(BODDI)H$_2$** in various metalation reactions aiming to access the related lithium, magnesium, calcium, and zinc complexes. The results are discussed below.

The reaction of **(BODDI)H$_2$** with *n*-butyllithium in a 1 : 1 ratio gives rise to a mixture of products presumably of both the mono- and dinuclear complex. Despite repeated attempts and altering the reaction conditions (order and speed of the addition, temperature) we could not reproducibly isolate the mononuclear complex. However, when the reaction is performed in a 1 : 2 stoichiometry of **(BODDI)H$_2$** and *n*-butyllithium, the dinuclear lithium complex **(BODDI)Li$_2$** is obtained as a red powder in 70% yield, Scheme 1. Several techniques (temperature, diffusion, solvent mixtures) were tested to obtain single crystals suitable for an X-ray diffraction analysis but remained unsuccessful. Nevertheless, the chemical integrity was established by ^{1}H and ^{13}C NMR as well as IR spectroscopy, Fig. S1–S3. The ^{1}H NMR resonance pattern of the ligand backbone, *i.e.*, one methyl and one methine singlet and of the 2,6-diisopropyl-phenyl (Dipp) groups (two methyl doublets and one multiplet accounting for the methine protons) is indicative for a symmetric or averaged structure in solution (C_6D_6). In line with a dinuclear complex, the absence of NH groups is evidenced by ^{1}H NMR and IR spectroscopy. To elucidate the molecular structure of **(BODDI)Li$_2$** in solution, diffusion-ordered (DOSY) ^{1}H NMR measurements have been performed (Fig. S4). Only a single major compound could be detected in solution, and its apparent molecular weight (1719 g mol^{-1}) corresponds more closely to a tetramer (calc. mol weight 1890 g mol^{-1}) than a dimer (calc. mol weight 945 g mol^{-1}) or a monomer (calc. mol weight 473 g mol^{-1}). Aggregation of lithium complexes is well known[11] and in lithium β-diketiminates for example, secondary interactions with aromatic carbons of neighbouring molecules can be involved.[12] Given the steric strain imposed by the BODDI ligand, we assume that related secondary interactions are also involved in the tetramerization of **(BODDI)Li$_2$**.

We next became interested in the related magnesium complexes and treated the protio-ligand **(BODDI)H$_2$** with Mg(HMDS)$_2$·(thf)$_2$ (HMDS: N(SiMe$_3$)$_2$), Mg(HMDS)$_2$, and MgEt$_2$·dioxane, respectively, Scheme 2. The mononuclear complex **(BODDI)H(MgHMDS)** is obtained from a 1 : 1 mixture of **(BODDI)H$_2$** and Mg(HMDS)$_2$·(thf)$_2$ in either benzene or THF within three hours in 54% yield. A 1 : 2 stoichiometry does not give rise to a second deprotonation even when heated to 60 °C for several days in C_6D_6. Using unsolvated Mg(HMDS)$_2$ instead allows for the isolation of three different products depending on the reaction conditions and the stoichiometry. A 1 : 1 mixture of **(BODDI)H$_2$** and Mg(HMDS)$_2$ in THF also affords the mononuclear complex **(BODDI)H(MgHMDS)** in 28% yield most likely due to the initial formation of Mg(HMDS)$_2$·(thf)$_2$. In toluene, however, two different dinuclear complexes are formed depending on the stoichiometry and the reaction conditions: using a 1 : 2.2 stoichiometry and performing the reaction at low temperature, *i.e.*, going from −196 °C to room temperature, affords the dinuclear heteroleptic complex **(BODDI)(MgHMDS)$_2$** in 41% crystalline yield. In contrast, using a 1 : 1 stoichiometry at 90 °C affords the dinuclear homo-

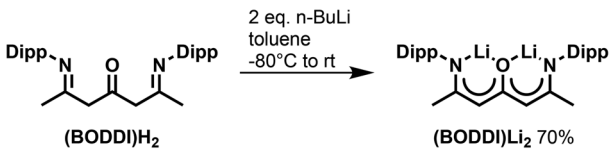

Scheme 1 Deprotonation of **(BODDI)H$_2$** affords the dinuclear lithium complex **(BODDI)Li$_2$**.

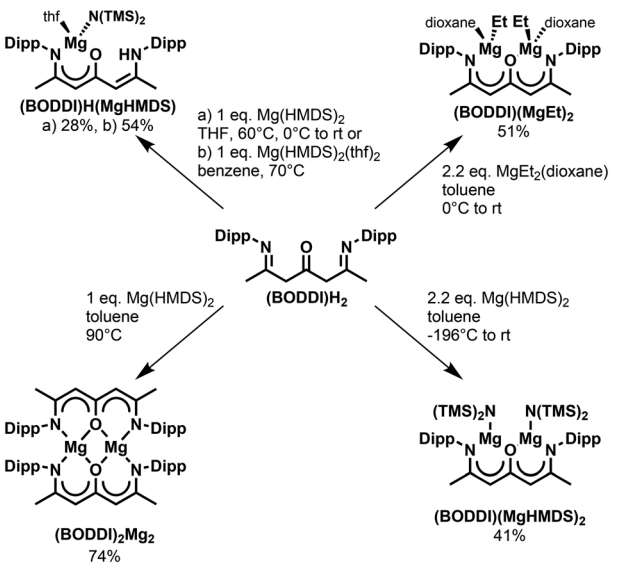

Scheme 2 Synthesis of mono- and dinuclear magnesium complexes starting from **(BODDI)H$_2$**.

Open Access Article. Published on 09 October 2025. Downloaded on 4/7/2026 7:46:47 PM.
This article is licensed under a Creative Commons Attribution 3.0 Unported Licence.

leptic complex **(BODDI)$_2$Mg$_2$** in 74% crystalline yield. These findings illustrate well the crucial role of the reaction conditions when ditopic ligands are applied. Notably, the selective formation of a mononuclear complex in which a second coordination side remains available is of high value for the subsequent synthesis of heterobimetallic complexes.

A mononuclear complex might also be formed in the reaction of **(BODDI)H$_2$** and $MgEt_2$·dioxane as indicated by the respective NH and γ-CH resonances in the crude ^{1}H NMR spectrum, but repeated attempts to obtain the respective mononuclear complex remained unsuccessful. However, the dinuclear complex **(BODDI)(MgEt)$_2$** was isolated in 51% yield from the reaction of the protio-ligand with two equivalents of $MgEt_2$·dioxane.

(BODDI)H(MgHMDS), **(BODDI)(MgHMDS)$_2$**, **(BODDI)$_2$Mg$_2$** as well as **(BODDI)(MgEt)$_2$** were obtained as single-crystals, which were investigated by X-ray diffraction analysis. In case of **(BODDI)(MgEt)$_2$**, the data were of poor quality and do not allow for a detailed discussion of structural parameters. However, the connectivity of the atoms was unambiguously established, Fig. S5, and agrees with the IR and NMR spectroscopic data, Fig. S6–S8.

(BODDI)H(MgHMDS) crystallizes as a monomeric complex in which the magnesium is coordinated by an HMDS-ligand, a molecule of THF and one of the two N,O binding pockets of the BODDI ligand in an overall distorted tetrahedral environment (Fig. 2a). The Mg–N and Mg–O bond lengths of 2.0689(17) and 1.9197(17) Å, respectively, within the $MgNC_3O$-metallacycle resemble values of homoleptic ketiminate complexes.[13] The NH proton could be located and refined isotropically. It forms a hydrogen bond to O1 inducing an overall almost planar arrangement of the BODDI framework as previously reported for related mononuclear nickel complexes.[10c]

The two distorted-trigonal coordinated magnesium centres in **(BODDI)(MgHMDS)$_2$** reside 0.65 Å (Mg1) and 0.70 Å (Mg2) above and below the almost planar BODDI backbone (Fig. 2b), a feature reminiscent of related dinuclear ethyl zinc complexes.[10a] The exocyclic Mg–N lengths resemble values of tricoordinated magnesium centres in previously reported mono- and dinuclear bis(trimethylsilyl)amide complexes.[14] Within **(BODDI)$_2$Mg$_2$**, two BODDI ligands are winded around two tetracoordinated magnesium centres forming a screw-shaped homoleptic structure with helical chirality (Fig. 2c). However, as **(BODDI)$_2$Mg$_2$** crystallizes in the centrosymmetric *C*2/*c* space group, both enantiomers are present in the crystal lattice. Compared to **(BODDI)(MgHMDS)$_2$**, the endocyclic Mg–O (1.967(0) to 1.9727(16) Å *versus* 1.9533(15) to 1.9541(14) Å) and Mg–N (2.082(3) to 2.091(2) Å *versus* 2.0089(19) to 2.0099(16) Å) bond lengths are slightly longer and the BODDI backbone deviates significantly from planarity because of the overall steric constraints. Furthermore, the Mg···Mg distance is substantially smaller for **(BODDI)$_2$Mg$_2$** (3.1169(15) Å) compared to **(BODDI)(MgHMDS)$_2$** (3.4882(9) Å).

Compared to their magnesium congeners, the more polar organocalcium compounds usually possess a higher reactivity towards organic substrates but Schlenk-type ligand exchange processes also become more pronounced for heavier alkaline-earth metal complexes.[14b,15] Hence, the synthesis of stable heteroleptic complexes might be a challenge, which is even pronounced in case of ditopic ligands.[14b] We investigated the reactivity of **(BODDI)H$_2$** with $Ca(HMDS)_2$·$(thf)_2$ [16] and dibenzyl calcium,[17] respectively, Scheme 3. Like the findings reported above for magnesium, $Ca(HMDS)_2$·$(thf)_2$ gives rise to the mononuclear heteroleptic complex **(BODDI)H(CaHMDS)**, which contains two molecules of THF according to the ^{1}H NMR spectrum, Fig. S9, in 53% crystalline yield. Again, the reaction conditions are crucial, and the reaction must be performed at low temperature, *i.e.*, from 0 °C to room temperature, to avoid subsequent reactions towards the dinuclear homoleptic complex **(BODDI)$_2$Ca$_2$**, which in contrast to its magnesium relative contains two molecules of THF. The latter is obtained in 74% crystalline yield when a benzene solution of **(BODDI)H(CaHMDS)** is heated to 80 °C for two hours. The reaction of **(BODDI)H$_2$** with dibenzyl calcium affords the heteroleptic dinuclear complex **(BODDI)(CaBn)$_2$**. Its ^{1}H NMR spectrum, Fig. S10, features a simple set of ^{1}H NMR resonances, *i.e.*, one doublet and one septet for the Dipp methyl and methine protons, indicating a symmetric or averaged structure

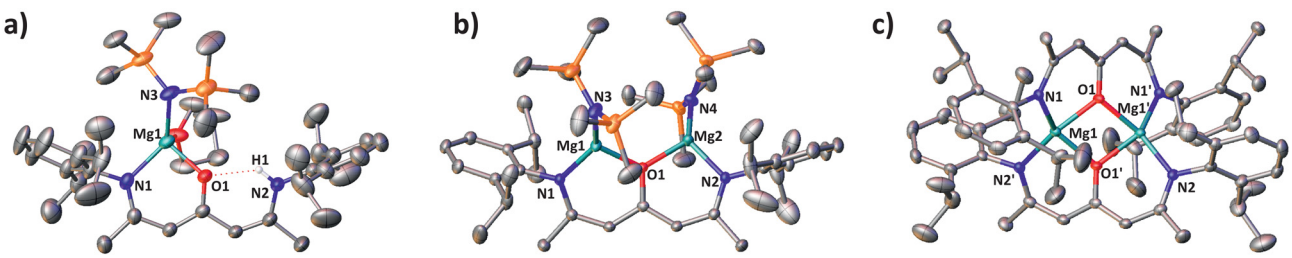

Fig. 2 Solid-state molecular structures (hydrogen atoms except the NH in **(BODDI)H(MgHMDS)** are omitted for the sake of clarity) with selected bond lengths [Å] and angles [°]. (a) **(BODDI)H(MgHMDS)**: Mg1–N1 2.0689(17), Mg1–N3 1.992(2), Mg1–O1 1.9197(17), O1···H1 2.05(2), N1–Mg1–O1 93.19(7), N1–Mg1–N3 130.92(8), N3–Mg1–O1 118.40(7). (b) **(BODDI)(MgHMDS)$_2$**: Mg1···Mg2 3.4882(9), Mg1–N1 2.0099(16), Mg1–N3 1.9471(17), Mg2–N2 2.0089(19), Mg2–N4 1.945(2), Mg1–O1 1.9533(15), Mg2–O1 1.9541(14), N1–Mg1–O1 97.61(7), N1–Mg1–N3 134.10(8), N3–Mg1–O1 124.80(7), N2–Mg2–O1 97.11(7), N2–Mg2–N4 137.55(8), N4–Mg2–O1 123.66(8). (c) **(BODDI)$_2$Mg$_2$**: Mg1···Mg1′ 3.1169(15), Mg1–N1 2.091(2), Mg1–N2′ 2.082(3), Mg1–O1 1.9727(16), Mg1–O1′ 1.9670(16), N1–Mg1–O1 87.44(8), N2′–Mg1–O1′ 88.32(8); symmetry transformations used to generate equivalents atoms (marked with ′): 1 – *x*, +*y*, 3/2 – *z*.

This journal is © The Royal Society of Chemistry 2025

Open Access Article. Published on 09 October 2025. Downloaded on 4/7/2026 7:46:47 PM.
This article is licensed under a Creative Commons Attribution 3.0 Unported Licence.

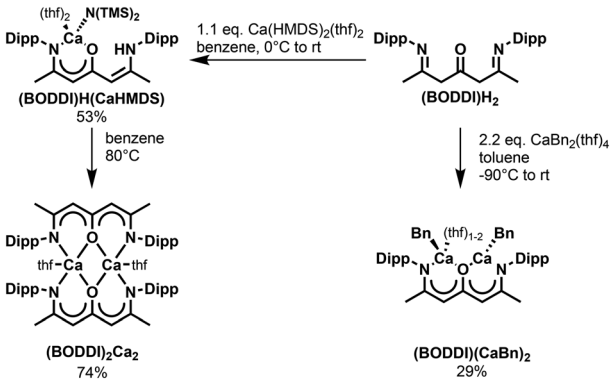

Scheme 3 Synthesis of mono- and dinuclear calcium complexes starting from **(BODDI)H$_2$**.

in solution. Furthermore, the coordination of one molecule of THF is evidenced by two characteristic multiplet resonances.

We were able to grow single crystals for all three compounds, which allowed us to establish their molecular solid-state structures by means of X-ray diffraction analysis, Fig. 3. Like **(BODDI)H(MgHMDS)**, **(BODDI)H(CaHMDS)** (Fig. 3a) crystallizes as a monomeric complex. However, due to the increased ionic radius of calcium compared to magnesium, the coordination of two molecules of THF gives rise to the higher coordination number six, commonly observed for calcium. The endocyclic Ca–N and Ca–O bond lengths of 2.472 (4) and 2.225(3) Å resemble values of homoleptic calcium ketiminate complexes[18] and the exocyclic Ca–N(HMDS) and Ca–O (thf) bonds are comparable with those of a THF-solvated calcium HMDS β-diketiminate complex.[19] Like **(BODDI)$_2$Mg$_2$** but impacted by the coordination of two additional THF molecules, *i.e.*, one per calcium atom, **(BODDI)$_2$Ca$_2$** (Fig. 3b) features helical chirality but crystallizes also in a centrosymmetric space group ($P\bar{1}$). The Ca–N bonds are slightly shorter than those in **(BODDI)H(CaHMDS)**, while the endocyclic Ca–O bonds are comparable. In case of **(BODDI)(CaBn)$_2$**, depending on the solvent used for crystallization two kinds of crystals could be obtained and analyzed, these are denoted **(BODDI)(CaBn)$_2$_a** (Fig. 3c) and **(BODDI)(CaBn)$_2$_b** (Fig. 3d). Both complexes feature two calcium(II) centres in different coordination environments but vary in the number of coordinated THF molecules, *i.e.*, one or two. Coordination of THF originates from Ca1, which features – besides being chelated by one of the two N,O-binding pockets – two calcium–carbon σ bonds. In contrast, Ca2 features only two σ bonds towards the nitrogen and oxygen atoms of the BODDI framework and additionally calcium–carbon π bonds with the two benzyl rests. The latter is expressed by η^6 coordination to one of the benzylic phenyl ring as well as binding of the second benzyl substituent in a η^3 fashion through C39, C44, and C45, Fig. 3c and d. While the connectivity is the same for both **(BODDI)(CaBn)$_2$_a** and **(BODDI)(CaBn)$_2$_b**, bonding of an additional molecule of THF in case of the latter impacts on some of the Ca–C and also the C–N bonds. The higher coordination number of calcium in **(BODDI)(CaBn)$_2$_b** causes longer Ca–N bonds. While the effect is significantly more pronounced at Ca1 it is still measurable for the Ca2–N2 bond. A similar situation is present for the Ca–C bonds: the two Ca1–C σ bonds are substantially longer for **(BODDI)(CaBn)$_2$_b** (Ca1–C38 2.666(2) Å, Ca1–C45 2.833(2) Å) as compared to **(BODDI)(CaBn)$_2$_a** (Ca1–C38 2.561(3) Å, Ca1–C45 2.658(3) Å), while in case of the Ca2–C39 and Ca2–C44 π bonds an elongation is measurable but much smaller. Finally, the distances between Ca2 and the C$_6$-perimeter are comparable with values of 2.4552(14) Å and 2.4594(11) Å for **(BODDI)(CaBn)$_2$_a** and **(BODDI)(CaBn)$_2$_b**, respectively.

Finally, we investigated the synthesis of dinuclear zinc β-oxo-δ-diiminate complexes. While the dinuclear complex **(BODDI)(ZnEt)$_2$** has previously been reported by Coates and co-workers,[10a] we wondered if the related mononuclear complex **(BODDI)H(ZnEt)** as well as the mono- and dinuclear bis(trimethylsilyl)amide zinc complexes are accessible as well.

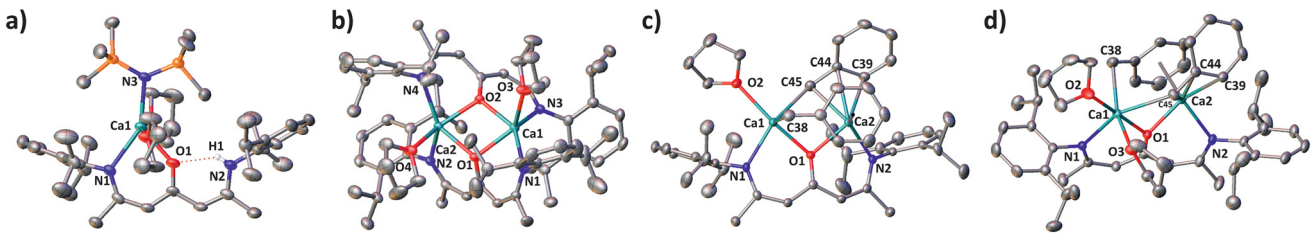

Fig. 3 Solid-state molecular structures (hydrogen atoms except the NH in **(BODDI)H(CaHMDS)** and non-coordinated solvent molecules are omitted for the sake of clarity) with selected bond lengths [Å] and angles [°]. (a) **(BODDI)H(CaHMDS)**: Ca1–N1 2.472(4), Ca1–N3 2.345(3), Ca1–O1 2.225(3), O1···H1 2.00(7), N1–Ca1–O1 77.40(13), N1–Ca1–N3 148.85(14), N3–Ca1–O1 133.70(12). (b) **(BODDI)$_2$Ca$_2$**: Ca1···Ca2 3.6011(12), Ca1–N1 2.437(3), Ca1–N3 2.418(3), Ca2–N2 2.416(3), Ca2–N4 2.412(3), Ca1–O1 2.270(3), Ca1–O2 2.262(3), Ca1–O3 2.387(3), Ca2–O1 2.245(3), Ca2–O2 2.298(3), Ca2–O4 2.388(3), N1–Ca1–O1 76.69(10), N2–Ca2–O1 80.79(10), N3–Ca1–O2 80.16(10), N4–Ca2–O2 77.02(10); (c) **(BODDI)(CaBn)$_2$_a**: Ca1···Ca2 3.3815(7), Ca1–N1 2.347(2), Ca2–N2 2.324(2), Ca1–O1 2.2641(17), Ca1–O2 2.388(2), Ca2–O1 2.2591(19), Ca1–C38 2.561(3), Ca1–C45 2.658(3), Ca2–C39 2.741(3), Ca2–C44 2.751(3), Ca2–C45 2.641(3), N1–Ca1–O1 79.19(7), N1–Ca1–O2 105.86(2), N2–Ca2–O1 79.77(7); (d) **(BODDI)(CaBn)$_2$_b**: Ca1···Ca2 3.4504(6), Ca1–N1 2.4340(16), Ca2–N2 2.3605(16), Ca1–O1 2.2639(13), Ca1–O2 2.3987(15), Ca1–O3 2.3891(15), Ca2–O1 2.2412(13), Ca1–C38 2.666(2), Ca1–C45 2.833(2), Ca2–C39 2.755(2), Ca2–C44 2.791(2), Ca2–C45 2.620(2), N1–Ca1–O1 79.35(5), N1–Ca1–O2 102.96(5), N2–Ca2–O1 82.84(5).

Open Access Article. Published on 09 October 2025. Downloaded on 4/7/2026 7:46:47 PM.
This article is licensed under a Creative Commons Attribution 3.0 Unported Licence.

Hence, the protio-ligand **(BODDI)H$_2$** was treated with diethyl zinc and Zn(HMDS)$_2$, respectively, Scheme 4. The reaction with zinc(II) bis[bis(trimethylsilylamide)] occurs smoothly and affords, depending on the stoichiometry and the reaction conditions, both the mononuclear complex **(BODDI)H(ZnHMDS)** and the dinuclear complex **(BODDI)(ZnHMDS)$_2$** in good crystalline yield, *i.e.*, 54% and 74%, respectively. A low field resonance (10.75 ppm) in the ^{1}H NMR spectrum of **(BODDI)H(ZnHMDS)**, Fig. S11, evidences the presence of an NH function as observed in case of the related magnesium (9.82 ppm) and calcium (10.22 ppm) complexes discussed above. In addition, two γ-CH resonances as well as two doublets of doublets and two multiplets accounting for the respective methyl and methine protons of the Dipp groups indicate a different environment of the two binding sites of the BODDI framework. In contrast and as expected for a homodinuclear complex, the ^{1}H and ^{13}C NMR spectra of **(BODDI)(ZnHMDS)$_2$** (Fig. S12 and S13) are reminiscent of a molecule with higher symmetry or molecular averaging on the NMR time scale.

Following the procedure of Coates and co-workers,[10a] **(BODDI)(ZnEt)$_2$** is readily available in 78% yield upon heating a 1 : 2.2 mixture of **(BODDI)H$_2$** and diethyl zinc. Using the same stoichiometry but performing the reaction at room temperature allowed for the isolation of the mononuclear complex **(BODDI)H(ZnEt)** in 61% yield. Again, a downfield-shifted singlet resonance (10.94 ppm) assigned to the amine proton along with two resonances accounting for two different γ-CH protons support the presence of a mononuclear complex with an empty enamine pocket, Fig. S14.

Single crystals could be obtained for **(BODDI)H(ZnHMDS)** and **(BODDI)(ZnHMDS)$_2$** as well as **(BODDI)(ZnEt)$_2$**. The molecular solid-state structures of the two bis(trimethylsilyl)amide zinc complexes have been investigated using X-ray diffraction

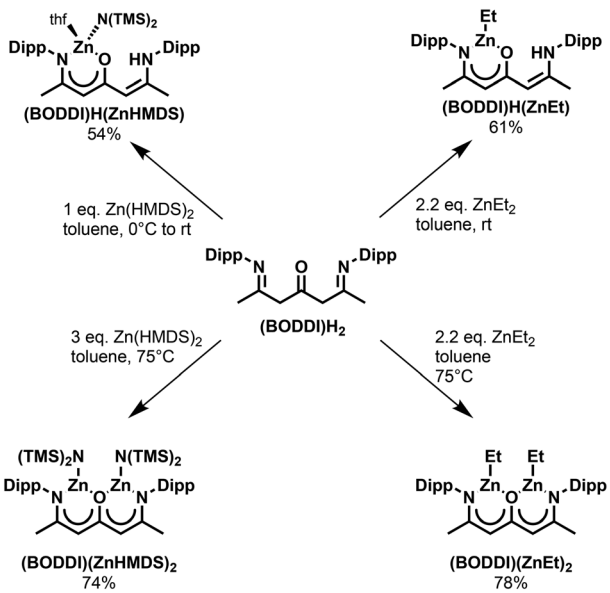

Scheme 4 Synthesis of mono- and dinuclear zinc complexes starting from **(BODDI)H$_2$**.

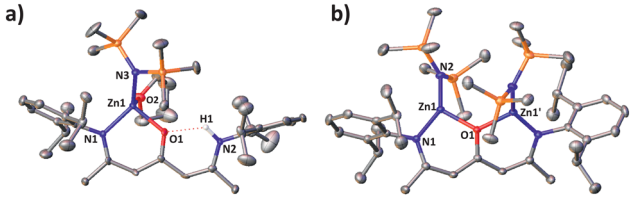

Fig. 4 Solid-state molecular structures (hydrogen atoms except the NH in **(BODDI)H(ZnHMDS)** and non-coordinated solvent molecules are omitted for the sake of clarity) with selected bond lengths [Å] and angles [°]. (a) **(BODDI)H(ZnHMDS)**: Zn1–N1 1.991(4), Zn1–N3 1.898(5), Zn1–O1 1.985(4), Zn1–O2 2.166(6), O1···H1 2.05(7), N1–Zn1–O1 96.97 (16), N1–Zn1–N3 129.4(2), N3–Zn1–O1 119.2(2). (b) **(BODDI)(ZnHMDS)$_2$**: Zn1···Zn1′ 3.5581(9), Zn1–N1 1.9303(19), Zn1–N2 1.8714(18), Zn1–O1 1.9926(10), Zn1′–N1′ 1.9303(19), Zn1′–N2′ 1.8714(18), Zn1′–O1 1.9926 (10), N1–Zn1–O1 95.62(6), N1–Zn1–N2 143.52(7), N2–Zn1–O1 120.33 (2), N1′–Zn1′–O1 95.62(6), N1′–Zn1′–N2′ 143.52(7), N2′–Zn1′–O1 120.33 (2); symmetry transformations used to generate equivalents atoms (marked with ′): 1 – *x*, +*y*, 1/2 – *z*.

analysis, Fig. 4, while the structure of **(BODDI)(ZnEt)$_2$** has been reported before.[10a] The structures of **(BODDI)H(ZnHMDS)** and **(BODDI)(ZnHMDS)$_2$** are reminiscent of their magnesium relatives **(BODDI)H(MgHMDS)** and **(BODDI)(MgHMDS)$_2$** discussed above. Both mononuclear complexes features NH···O hydrogen bonds of comparable length. When comparing the mono- and dinuclear zinc complexes, similar Zn–O but different Zn–N bond lengths are recognized. Due to the decrease of the coordination number of zinc from four to three, the endocyclic Zn–N bonds get significantly shorter (1.991(4) *vs.* 1.9303(19) Å) and resemble values reported for **(BODDI)(ZnEt)$_2$** [10a] and dinuclear bis(trimethylsilyl)amide zinc complexes based on bis(β-diketiminate)s.[20]

Ring-opening polymerization of L-lactide

The capability of the complexes discussed above and the previously reported magnesium hydride complex **(BODDI)(MgH)$_2$** [21] to initiate the ring-opening polymerization (ROP) was tested using L-lactide (LLA) without the use of an additional activator, Table 1. The results have been analyzed with respect to the activity but also the structure of the thus formed polylactide. For comparison, the very potent initiator **NacNacMgHMDS** [22] and the previously reported **AcNacMgHMDS**,[23] Fig. 5, were synthesized as well and were subsequently used as a reference for the other experiments. A catalyst–monomer ratio of 1 : 200 for the dinuclear complexes was applied while in case of the mononuclear complexes ratios of 1 : 100 as well as 1 : 200 were tested. In a typical experiment, a LLA solution (0.4 mol L^{-1}) in THF was treated with the related complex at 30 °C ± 1.9 °C and the reaction progress was monitored using *in situ* IR spectroscopy. At 60% conversion, a part of the reaction mixture was quenched by adding a 1 M solution of hydrochloric acid in methanol and the formed polymer was precipitated using methanol. The obtained material was characterized with respect to its dispersity (*Đ*) and the number average molecular weight M_n by size-exclusion

This journal is © The Royal Society of Chemistry 2025

Open Access Article. Published on 09 October 2025. Downloaded on 4/7/2026 7:46:47 PM.
This article is licensed under a Creative Commons Attribution 3.0 Unported Licence.

Table 1 Catalytic data for the ROP of L-lactide. Conversions were deduced from *in situ* IR spectroscopy. Reaction conditions: room temperature, THF, monomer concentration 0.4 mol L^{-1}, SEC data was obtained by calibration with PMMA standards in $CHCl_3$/i-PrOH/NEt_3 94 : 2 : 4

Entry	Cat	Cat : mon ratio	$t_{60\%}$ [a] [min]	$Đ$ SEC (M_w/M_n)	M_n SEC (g mol^{-1})	t_{total} [b] [min]	$Đ$ SEC (M_w/M_n)	M_n SEC (g mol^{-1})
1	**NacNacMgHMDS**	1 : 100	0.14	1.62	3.51×10^4	2 (86%)	1.67	3.39×10^4
2	**NacNacMgHMDS**	1 : 200	—	—	—	13 (56%)	1.61	3.87×10^4
3	**AcNacMgHMDS**	1 : 200	18.09	—	—	—	—	—
4	**(BODDI)H_2**	1 : 200	—	—	—	—	—	—
5	**(BODDI)H(MgHMDS)**	1 : 100	0.51	1.41	1.48×10^5	2.25 (99%)	1.61	1.52×10^5
6	**(BODDI)H(MgHMDS)**	1 : 200	0.68	1.29	1.92×10^5	3.9 (99%)	1.64	2.13×10^5
7	**(BODDI)H(CaHMDS)**	1 : 100	4.01	1.54	2.28×10^4	30 (66%)	1.63	2.16×10^4
8	**(BODDI)H(CaHMDS)**	1 : 200	—	—	—	32 (45%)	1.67	2.74×10^4
9	**(BODDI)H(ZnHMDS)**	1 : 100	10.18	1.42	1.24×10^5	45 (99%)	1.49	1.57×10^5
10	**(BODDI)H(ZnHMDS)**	1 : 200	18.01	1.51	1.28×10^5	60 (95%)	1.61	1.41×10^5
11	**(BODDI)H(ZnEt)**	1 : 200	—	—	—	—	—	—

[a] The reaction progress was monitored using *in situ* IR spectroscopy. $t_{60\%}$ refers to the reaction time required to reach 60% conversion. [b] Time at which the reaction was quenched, *i.e.*, when no further progress was observed.

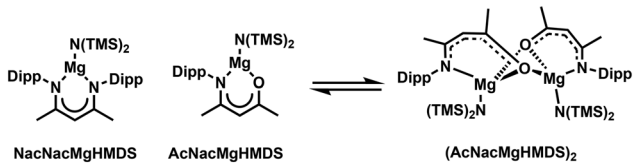

Fig. 5 Structural formulas of the reference complexes used in this study.

chromatography (SEC). In addition, the remaining reaction mixture was quenched at the end of the reaction (t_{total}) and analyzed as well. As expected, the protio-ligand **(BODDI)H_2** is catalytically inactive under the experimental conditions (ratio 1 : 200). Among the mononuclear catalysts **(BODDI)H(MHMDS)** with M = Mg, Ca, Zn, the magnesium complex is most active giving 60% conversion in 31 s (1 : 100) and 41 s (1 : 200). Hence, with the higher catalyst to monomer ratio, **(BODDI)H(MgHMDS)** outperforms **NacNacMgHMDS**, which gave only 56% conversion after 13 minutes. However, in case of a 1 : 100 ratio, **NacNacMgHMDS** is the faster initiator giving 60% conversion within only 8 seconds. In comparison, **AcNacMgHMDS** [23] (1 : 200) is much slower and requires about 18 minutes to convert 60% of the monomer; a similar value was observed for **(BODDI)H(ZnHMDS)**. The reactivity trends observed for **NacNacMgHMDS** and **AcNacMgHMDS** can be explained by the different donor properties and aggregation behaviour of the supporting ligands. The NacNac (N,N) ligand framework provides strong σ-donation, leading to an electron-rich but coordinatively labile magnesium centre. This results in a higher propensity for substrate activation compared to the AcNac (N,O) analogue. In the latter, the oxygen donor withdraws more electron density, rendering magnesium more electron-deficient, but at the same time stabilizes dimeric structures, as has been reported in the literature.[23] The predominance of such aggregated compounds effectively reduces the number of accessible active sites. In comparison, **(BODDI)H(MgHMDS)** exhibits the highest catalytic activity. The β-oxo-δ-diimine ligand enforces a less electron-rich magnesium centre, enhancing its Lewis acidity, while remaining monomeric under the reaction conditions. The coexistence of a more electrophilic, yet accessible active site explains the superior performance of the BODDI complex relative to both NacNac and AcNac derivatives. In the case of **(BODDI)H(CaHMDS)** a conversion of only 45% was found after 32 minutes. Besides the catalytic activity, the properties of the polymers are also different. Again, **(BODDI)H(MgHMDS)** gives the best result: the sample obtained at 60% conversion for the 1 : 200 catalyst : monomer ratio features a narrow $Đ$ of 1.29 and an M_n of 1.92×10^5 g mol^{-1}. Allowing the reaction to run to full conversion gives a material with a higher $Đ$ of 1.64 along with a slightly higher M_n of 2.13×10^5 g mol^{-1}. Notably, the values for the material obtained with a 1 : 100 ratio at 60% conversion are to some extent poorer, *i.e.*, higher $Đ$ of 1.41 and lower M_n of 1.48×10^5 g mol^{-1} but still outperform those found for **NacNacMgHMDS** under the same experimental conditions. The same trend discussed for the catalytic activity is also observed for the polymer properties and the number average molecular weight decreases in going from Mg to Zn and finally Ca, while at the same time the dispersity increases in that order. Notably, **(BODDI)H(ZnEt)** is inactive under the experimental conditions.

The dinuclear complexes were all probed at a catalyst : monomer ratio of 1 : 200 and illustrate well the impact of both the metal and the second ligand on the catalytic performance. **(BODDI)Li_2** and the heteroleptic magnesium complexes **(BODDI)$(MgHMDS)_2$** and **(BODDI)$(MgEt)_2$** cause a fast initiation leading to 60% conversion within a minute or less. Among this triple, **(BODDI)$(MgEt)_2$** is the fastest and needs only 6 seconds followed by the dinuclear lithium complex and finally the dinuclear magnesium HMDS complex. The dispersities of the thus formed polymers follow the same trend. **(BODDI)Li_2** and **(BODDI)$(MgEt)_2$** give polymers of comparable relative number average molecular weights by size exclusion chromatography M_n of 2.79×10^4 and 2.74×10^4 g mol^{-1}, respectively, while the polymer obtained by **(BODDI)**

Open Access Article. Published on 09 October 2025. Downloaded on 4/7/2026 7:46:47 PM.
This article is licensed under a Creative Commons Attribution 3.0 Unported Licence.

(MgHMDS)$_2$ is about twice as large (M_n of 50 × 10^4 g mol^{-1}). The heteroleptic magnesium hydride complex **(BODDI)$_2$(MgH)$_4$** [21] as well as the homoleptic complex **(BODDI)$_2$Mg$_2$** require significantly more time. In the first case, a maximum of 42% conversion is reached after 60 minutes, while in the latter case 60% of the monomer are converted after about 9 minutes and 90% after 88 minutes. In both cases a material of comparable dispersity (1.39 *vs.* 1.47) but different molecular weight (M_n 3.08 × 10^4 *vs.* 5.30 × 10^4 g mol^{-1}) is obtained at the end of the reactions. Although **(BODDI)(CaBn)$_2$** does initiate the polymerization of L-lactide and gives 60% conversion after about 90 minutes, no product could be precipitated from the reaction mixture, which impedes further characterization. The homoleptic calcium complex **(BODDI)$_2$Ca$_2$** affords 58% conversion after 80 minutes giving a polymer with a reasonable dispersity of 1.43 but with the lowest M_n (2.67 × 10^4 g mol^{-1}) among the dinuclear complexes investigated in here. The heteroleptic zinc complex **(BODDI)(ZnHMDS)$_2$** is about 133-times slower than its magnesium counterpart **(BODDI)(MgHMDS)$_2$** but affords the material with the highest number average molecular weight of 6.14 × 10^4 g mol^{-1} in the series of dinuclear complexes at the end of the reaction. Finally, we found **(BODDI)(ZnEt)$_2$** to be inactive under the experimental conditions. We compared the mononuclear and dinuclear complexes **(BODDI)H(MgHMDS)** *vs.* **(BODDI)(MgHMDS)$_2$**, **(BODDI)H(CaHMDS)** *vs.* **(BODDI)(CaBn)$_2$**, and **(BODDI)H(ZnHMDS)** *vs.* **(BODDI)(ZnHMDS)$_2$**. For a fair comparison, the concentrations were adjusted to maintain a constant number of metal centres, *i.e.* 1 : 100 for the mononuclear complexes and 1 : 200 for the dinuclear complexes, respectively. Under these conditions, the mononuclear complexes consistently exhibited faster kinetics than their dinuclear analogues, although both systems generally reached high final conversions (89–99%). For the calcium complexes, the same kinetic trend was observed; however, the mononuclear complex reached only a maximum conversion of 66%, while the dinuclear analogue required 133.37 min to achieve 60% conversion (no higher value was determined). This behaviour is likely due to the improved accessibility of the active site in the mononuclear complexes, whereas in the dinuclear complex the proximity of the two metal centres and the more congested ligand environment may reduce the effective rate of monomer activation and insertion.

Mechanistic aspects by end-group analysis

To propose a conceivable mechanism, polymerization reactions with the selected catalysts (**(BODDI)(MgHMDS)$_2$** and **(BODDI)$_2$Mg$_2$** were conducted. To find out whether the monomer quality plays a significant role in the ROP, it was used as delivered (Table 3, entries 21 & 24) and after additional purification (recrystallized and sublimed twice, Table 3, entries 22 and 25). In the latter case, an additional experiment using 1-hexanol as a co-initiator (I) was conducted (Table 3, entries 23 & 26). Furthermore, with L-lactide used as delivered, benzyl alcohol was also tested as initiator (Table 3, entry 27). In this case, the reaction proceeded very rapidly, reaching 60% conversion within 30 seconds. When 1-hexanol was used instead, the polymerization was somewhat slower, which allowed sampling at lower conversions and thus enabled a more detailed end-group analysis. Matrix-assisted laser desorption/ionization time-of-flight mass spectrometry (MALDI-TOF MS) was used to investigate the end groups of the polymer chains and to provide insights into the mechanism of the ROP. Selected sections of the respective mass spectra for both catalysts are shown in Fig. 6, while the full MALDI-TOF MS spectra are provided in the SI (Fig. S15). The enlarged spectra show degrees of polymerization (DP) of 35 and 36. In all spectra, the signals (sodium adduct) of the main series are separated by 144 *m*/*z* units, which accounts for the molecular weight of a LA repeating unit. Both cyclic and linear polylactides are formed, regardless of whether raw or purified

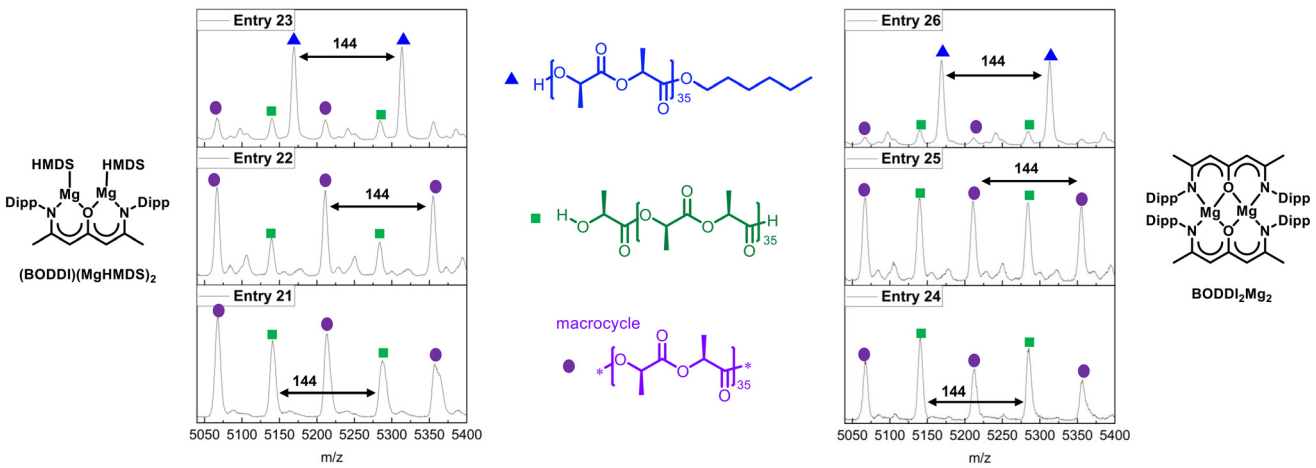

Fig. 6 Selected sections of the respective MALDI-TOF mass spectra of the poly(L-lactide)s obtained by polymerization of purchased and purified L-lactide in THF with **(BODDI)(MgHDMS)$_2$** (entries 21–23) and **(BODDI)$_2$Mg$_2$** (entries 24–26) as catalysts at room temperature (mon : cat = 200 : 1). Conditions: entries 21 and 24: purchased L-lactide, no initiator; entries 22 and 25: purified L-lactide, no initiator; entries 23 and 26: purified L-lactide, 1-hexanol as initiator. All samples were taken and quenched with HCl in methanol after a conversion of 20–40%.

This journal is © The Royal Society of Chemistry 2025

Open Access Article. Published on 09 October 2025. Downloaded on 4/7/2026 7:46:47 PM. This article is licensed under a Creative Commons Attribution 3.0 Unported Licence.

L-lactide is used. The formation of cyclic oligomers indicates that intramolecular transesterification occurred. The presence of HMDS as end groups in the polymer chains, in the case of **(BODDI)(MgHMDS)$_2$**, can be ruled out based on the results of the MALDI-TOF mass spectra. When using 1-hexanol as a co-initiator (Table 3, entries 23 & 26), formation of cyclic polylactide is suppressed and this effect is more pronounced for **(BODDI)$_2$Mg$_2$** compared to **(BODDI)(MgHMDS)$_2$**. The use of 1-hexanol as initiator predominantly afforded linear polylactide, enabling effective control over the polymerization, ^{1}H NMR spectroscopy was also used to determine end-groups and absolute number-average molar mass $M_{n,NMR}$ of the polymer. Details on the calculation of the number average degree of polymerization $DP_{n,NMR}$, its comparison with theoretical $DP_{n,cal}$ values, and the resulting initiator efficiency (f) are provided in the SI (Tables S2 and S3). Fig. 7 shows the stacked ^{1}H NMR spectra of entries 21 and 23 (Table 3). The methine (C*H*) protons of the linear and cyclic polymer feature different chemical shifts (5.14–5.18 ppm) compared to the monomer L-lactide (5.02–5.05 ppm).[24] The signal at 4.35 ppm can be assigned to the methine end-group (C*H*, *z1*) and its integral fits well with the integral of the respective hydroxy group (d, 2.63 ppm) (Fig. S16). Due to coupling of the methine proton with both the methyl and hydroxy moiety, the methine resonance of this end-group (C*H*, z1) appears as a quintet. The coupling is experimentally supported by the addition of D_2O (Fig. S17), which caused H/D exchange and a change of the multiplicity of the methine group from a quintet to a quartet. Furthermore, the disappearance of the hydroxy resonance (doublet) at 2.63 ppm was observed as well. However, the integral of the methine proton of the end-group is very low (<1%), which is why it can be assumed that the cyclic polylactide is formed as the main product in which such a group is absent.[25] It is therefore not possible to reliably differentiate between linear and cyclic structures based on the ^{1}H-NMR spectrum. With respect to the second end group of the linear polymer, the resonance at 3.76 ppm was attributed to a methoxy end-group,[26] and the signal at 11.97 ppm refers to a carboxyl group (Fig. S16); both originate from quenching the reaction with HCl in methanol. The ^{1}H NMR spectra of the polymers prepared with the purified L-lactide (entries 22 and 25) resemble those obtained with L-lactide that was used as delivered (Fig. S18). When 1-hexanol was used as an initiator (entries 23 and 26), new resonances in the ^{1}H NMR spectrum can be recognized in account for the hexanolate moiety (Fig. 7b). These include for example an additional multiplet (–O–CH_2) at 4.12 ppm (see also Fig. S19). The integrals of the hexanolate and hydroxyl end groups do not suggest a 1 : 1 ratio, which could be explained by partial cleavage of the hexanolate end group and its replacement by methoxy and carboxyl groups during the quenching step with HCl in methanol. Additionally, in the ^{1}H NMR spectra, no resonances indicative of *meso*- or D,D-units were observed, suggesting that epimerization is negligible under the experimental conditions used in here. We note, however, that epimerization has been reported under more forcing conditions, such as elevated temperatures

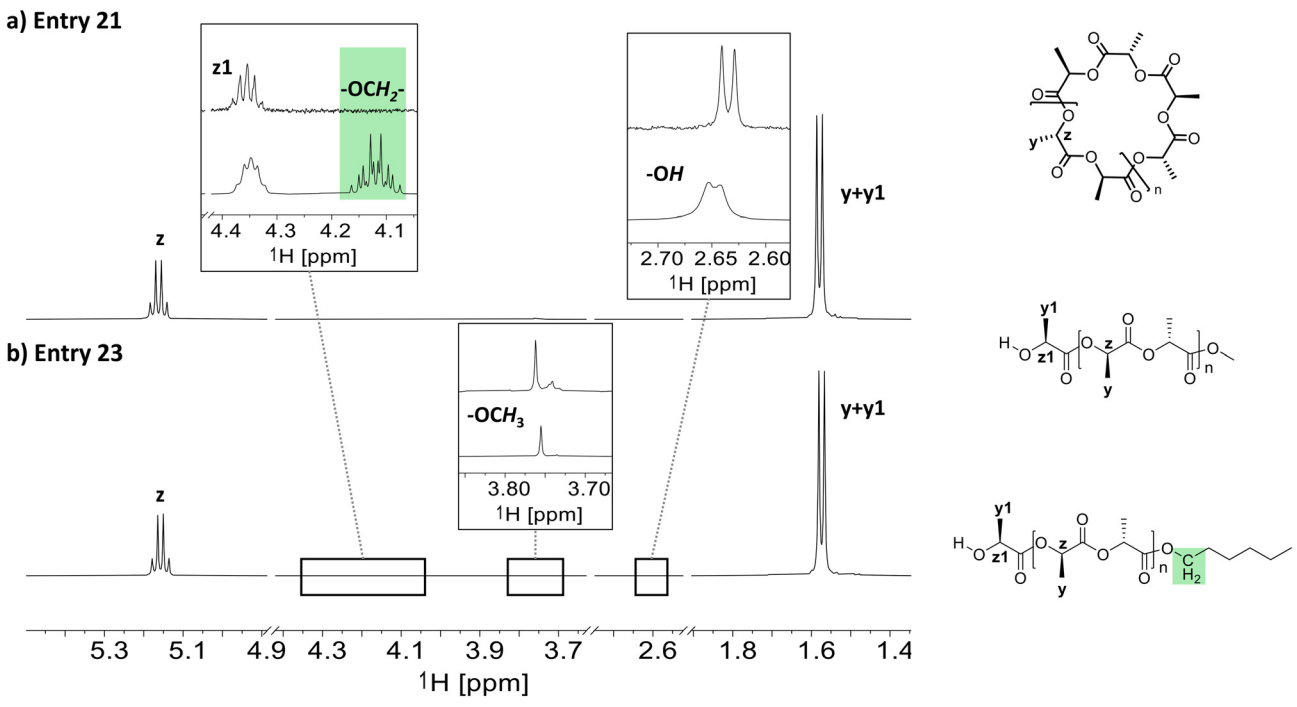

Fig. 7 Stacked sections of the ^{1}H NMR spectra ($CDCl_3$) of (a) entry 21 after 20–30% conversion and (b) entry 23 after 30–40% conversion of L-lactide to cyclic L-PLA and linear L-polylactide obtained with **(BODDI)(MgHMDS)$_2$** in THF at room temperature (mon : cat = 200 : 1). Cyclic polylactides have no terminal groups. It is therefore not possible to reliably differentiate between linear and cyclic structures based on the ^{1}H-NMR spectrum. The CH_2 group of the hexanolate, resulting from the used initiator 1-hexanol, is highlighted in green.

Open Access Article. Published on 09 October 2025. Downloaded on 4/7/2026 7:46:47 PM.
This article is licensed under a Creative Commons Attribution 3.0 Unported Licence.

or in the presence of strong organic bases such as, 5,7-triazabicyclo[4.4.0]dec-5-ene (TBD).[27] The MALDI-TOF spectra as well as the ^{1}H NMR spectra of the end-group analysis confirm the presence of both hexanolate and hydroxyl as end groups and in small quantities also methoxy and carboxyl groups.

Dinuclear magnesium ketodiiminate complexes are known to show an excellent reactivity and selectivity for the synthesis of cyclic polylactide.[28] In contrast, the dinuclear magnesium complexes **(BODDI)(MgHMDS)$_2$** and **(BODDI)$_2$Mg$_2$** reported in here display lower specificity, as both cyclic and linear polylactides are formed under the applied reaction conditions. Nevertheless, **(BODDI)(MgHMDS)$_2$** also achieves high conversions of 89% within only 1.94 minutes (entry 13). Based on the results of the end-group analysis and the MALDI-TOF spectra, it is proposed that the polymerization with both catalysts and with or without initiator proceeds *via* a coordination insertion mechanism (see SI, Schemes S1 and S2). In particular, the detection of alcohol end groups in both NMR and MALDI-TOF spectra suggests the presence of chain ends that are characteristic for a coordination–insertion pathway, whereas anionic polymerizations typically yield acyllactide end groups.[29]

Conclusions

In summary, we have reported the synthesis of mono- and dinuclear β-oxo-δ-diiminate (BODDI) complexes incorporating lithium, magnesium, calcium, and zinc, respectively, as well as their use for the ring-opening polymerization of L-lactide. Three mononuclear complexes **(BODDI)H(MHMDS)** with M being Mg, Ca or Zn could be isolated and structurally characterized. In case of the nine bimetallic complexes, the formation of hetero- or homoleptic complexes is strongly dependent on the metal and the metal source. While in case of zinc the respective heteroleptic complexes are readily available, formation of their magnesium and calcium analogs depends on the reaction conditions. Here, both hetero- and homoleptic complexes could be obtained. The catalytic activity of the complexes as well as the characteristics of the thereby formed polymers is strongly dependent on the metal, the number of metal atoms as well as the nature of the second ligand. The mononuclear complex **(BODDI)H(MgHMDS)** and the dinuclear complexes **(BODDI)Li$_2$**, **(BODDI)(MgHMDS)$_2$** as well as **(BODDI)(MgEt)$_2$** are fast initiators that give 60% conversion within a minute or less. As such, their catalytic performance competes or even outperforms **NacNacMgHMDS**. Furthermore, using **(BODDI)H(MgHMDS)** gives polylactide with a higher number average molecular weight M_n and a lower dispersity compared to **NacNacMgHMDS**. End-group analysis with MALDI-TOF mass spectrometry and ^{1}H NMR spectroscopy showed the formation of dominating cyclic L-polylactides *via* intramolecular transesterification reactions, especially in the absence of 1-hexanol as a co-initiator. In the presence of 1-hexanol, mostly linear chains are formed. The polymerization with the studied catalysts proceeds likely *via* a coordination-insertion mechanism.

Experimental section

General considerations

All preparations were performed under an inert atmosphere of dinitrogen by means of standard Schlenk-line techniques, while the samples for analytics were handled in a glovebox (MBraun). Yields have not been optimized and refer to isolated crystalline material. All solvents (toluene, *n*-pentane, *n*-hexane, tetrahydrofuran) were distilled from Na/benzophenone prior to use while 1-hexanol, benzyl alcohol, C_6D_6, THF-d_8 and toluene-d_8 were dried using molecular sieves (4 Å). **NacNacMgHMDS**,[22] **AcNacMgHMDS**,[23] **(BODDI)H$_2$**,[10a] **(BODDI)$_2$(MgH)$_4$**,[21] Mg(HMDS)$_2$,[30] Mg(HMDS)$_2$(thf)$_2$,[31] Mg(Et)$_2$(dioxane),[32] Ca(HMDS)$_2$(thf)$_2$,[16] Ca(Bn)$_2$(thf)$_4$,[17] and Zn(HMDS)$_2$ [33] were synthesized according to published procedures.

(BODDI)Li$_2$. A Schlenk-flask equipped with a stirring bar was charged with **(BODDI)H$_2$** (0.500 g, 1.09 mmol, 1 equiv.) and 4 mL toluene under inert conditions. A solution of ^{n}BuLi 2.5 M in *n*-hexane (0.9 mL, 2.28 mmol, 2.1 equiv.) was added dropwise at −80 °C. The solution was warmed up to room temperature and the solvent was removed under reduced pressure. The product was obtained as a red powder (0.360 g, 70%). ^{1}H NMR (300 MHz, C_6D_6): δ = 1.05 [br d, J = 6.80 Hz, 12 H, CH(CH_3)$_2$], 1.21 [d, J = 6.80 Hz, 12 H, CH(CH_3)$_2$], 1.62 [s, 6 H, –CH_3], 2.86–3.02 [m, 4 H, CH(CH$_3$)$_2$], 4.78 [s, 2 H, CH$_3$CNCH], 7.03–7.13 [m, 6 H, *Ar*]. ^{13}C NMR (75 MHz, C_6D_6): δ = 24.55, 25.11, 29.08, 91.90, 128.89, 129.67, 138.22, 141.50, 168.59, 178.22; IR(ATR): 3056 (w), 2960 (m), 2868 (m), 1467 (s), 1426 (s), 1398 (s), 1370 (vs), 1355 (vs), 1303 (vs), 1243 (s), 1215 (s), 1156 (vs), 1096 (s), 1049 (m), 1040 (m), 992 (s), 967 (s), 952 (m), 934 (s), 919 (s), 833 (m), 788 (s), 762 (s), 729 (s), 693 (m); elemental analysis calculated (found) $C_{31}H_{42}Li_2N_2O$: C 78.79 (77.89), H 8.96 (8.90), N 5.93 (5.24).

(BODDI)H(MgHMDS)

Method (a). A Schlenk-flask equipped with a stirring bar was charged with Mg(HMDS)$_2$ (1.498 g, 4.34 mmol, 1 equiv.) and 20 mL THF under inert conditions. The solution was stirred at 60 °C for 1 h and cooled to 0 °C. A solution of **(BODDI)H$_2$** (2 g, 4.34 mmol, 1 equiv.) in 10 mL THF was cooled to 0 °C and added to the reaction mixture. The solution was slowly warmed up to room temperature while stirring overnight. The solvent was removed under reduced pressure and the residue was washed with *n*-hexane followed by THF. Pale yellow, fine crystals were obtained (0.880 g, 28%). Crystals suitable for X-ray analysis were obtained by cooling a saturated solution in toluene to −30 °C.

Method (b). A Schlenk-flask equipped with a stirring bar was charged with Mg(HMDS)$_2$(thf)$_2$ (1.14 g, 2.33 mmol, 1.1 equiv.), **(BODDI)H$_2$** (1.06 g, 2.30 mmol, 1 equiv.) and 10 mL of benzene. The mixture was stirred at 70 °C for three hours before the solvents were removed under reduced pressure. The remaining residue was washed with *n*-hexane (3 times with 10 mL each). Pale yellow crystals were obtained (0.883 g, 54%) by recrystallization from benzene.

^{1}H NMR (400 MHz, C_6D_6) δ = 0.15 [s, 18H, Si(CH_3)$_3$], 1.16 [d, br, J = 6.14 Hz, 12H, –CH–(CH_3)$_2$], 1.21 [d, J = 6.14 Hz, 6H,

 This journal is © The Royal Society of Chemistry 2025

Open Access Article. Published on 09 October 2025. Downloaded on 4/7/2026 7:46:47 PM. This article is licensed under a Creative Commons Attribution 3.0 Unported Licence.

–CH–(CH_3)$_2$] 1.47–1.43 [m, 6H, –*THF*], 1.49 [s, 3H, –CH_3], 1.67 [s, 3H–CH_3], 3.32 [s, br, 2H, –*CH*–(CH_3)$_2$], 3.45–3.38 [m, 2H–*CH*–(CH_3)$_2$], 3.86–3.83 [m, 4H, –*THF*], 4.95 [s, 1H, –*H*], 5.07 [s, 1H, –*H*], 7.19–7.09 [m, 6H, –*ArH*] 9.82 [s, 1H, –*NH*]. ^{13}C NMR (151 MHz, C_6D_6) δ = 6.40 [–Si(CH_3)$_3$], 20.90 [–CH_3], 24.22 [–CH(CH_3)$_2$], 24.65 [–CH_3], 25.16 [–CH(CH_3)$_2$], 25.57 [–*THF*], 28.75 [–*CH*(CH_3)$_2$], 70.06 [–*THF*], 97.40 [–*CH*], 97.63 [–*CH*], 124.18 [–*m*-CH_{arom}], 124.52 [–*m*-CH_{arom}], 126.07 [–*p*-CH_{arom}], 135.41 [–i-C_{arom}], 142.62 [–*o*-C_{arom}], 146.05 [–i-C_{arom}], 147.93 [–*o*-C_{arom}], 155.00 [–*CN*], 172.33 [–*CN*], 182.09 [–*CO*]. ^{29}Si NMR (80 MHz, C_6D_6) δ = −8.71; IR(ATR): $\tilde{\nu}$ = 3060, 2958, 2870, 1616, 1498, 1461, 1435, 1392, 1362, 1318, 1269, 1249, 1236, 1210, 1165, 1098, 1055, 1027, 1005, 954, 934, 919, 876, 824, 794, 777, 760, 751, 734, 684, 662 cm^{-1}; elemental analysis calculated (found) $C_{41}H_{68}MgN_3OSi_2$: C 68.83 (68.19), H 9.58 (9.55), N 5.87 (5.60).

(BODDI)(MgHMDS)$_2$. A Schlenk-flask equipped with a stirring bar was charged with **(BODDI)H$_2$** (4 g, 8.68 mmol, 1 equiv.) and Mg(HMDS)$_2$ (6.591 g, 19.10 mmol, 2.2 equiv.) under inert conditions at rt. The flask was cooled to −196 °C and 80 mL toluene was added, which partly froze upon addition. The flask was warmed up to 0 °C und stirred for 18 h, followed by stirring at room temperature for 8 h. The solvent was removed under reduced pressure and the residue was refluxed with 80 mL *n*-hexane. The solution was filtered hot and the product crystallized from the solution at room temperature, resulting in crystals suitable for X-ray analysis. Crystallization further proceeded by cooling to −30 °C. Yellow, fluorescent, rhombic crystals were obtained (2.95 g, 41%). ^{1}H NMR (400 MHz, C_6D_6): δ = 0.19 [s, 36H, –Si(CH_3)$_3$], 1.17 [d, J = 6.72 Hz, 12H, –CH–(CH_3)$_2$], 1.41 [d, J = 6.72 Hz, 12H, –CH–(CH_3)$_2$], 1.55 [s, 6H, –CH_3], 3.22 [spt, J = 6.87 Hz, 4H, –*CH*–(CH_3)$_2$], 4.82 [s, 2H, –*H*], 7.14 [s, 6H, *Ar*]. ^{13}C NMR (100 MHz, C_6D_6): δ = 4.90 [–Si(CH_3)$_3$], 23.93 [–CH(CH_3)$_2$], 23.99 [–CH_3], 24.61 [–CH(CH_3)$_2$], 28.55 [–*CH*(CH_3)$_2$], 94.66 [–*CH*], 123.93 [–*m*-CH_{arom}], 125.98 [–*p*-CH_{arom}], 142.15 [–*o*-C_{arom}], 143.35 [–i-C_{arom}], 171.03 [–*CN*], 171.47 [–*CO*]; ^{29}Si NMR (80 MHz, C_6D_6): δ = −8.04; IR(ATR): $\tilde{\nu}$ = 3064, 2950, 2870, 1536, 1461, 1433, 1366, 1355, 1336, 1312, 1273, 1254, 1241, 1219, 1172, 1111, 1098, 1023, 988, 936, 923, 878, 857, 848, 839, 807, 796, 760, 751, 716, 703, 665 cm^{-1}; elemental analysis calculated (found) $C_{43}H_{78}Mg_2N_4OSi_4$: C 62.37 (61.54), H 9.49 (9.22), N 6.77 (6.37).

(BODDI)(MgEt)$_2$. Following a recently reported procedure,[21] a Schlenk-flask equipped with a stirring bar was charged with **(BODDI)H$_2$** (1 g, 2.17 mmol, 1 equiv.) and 20 mL toluene under inert conditions. A suspension of Mg(Et)$_2$(dioxane)$_2$ (1.235 g, 4.78 mmol, 2.2 equiv.) in 20 mL toluene was added dropwise at 0 °C. The solution was stirred at room temperature overnight. The product crystallizes from the reaction mixture at room temperature as fine needles (860 mg, 51%). Crystals suitable for X-ray analysis were obtained by recrystallization from hot 1,4-dioxane. ^{1}H NMR (400 MHz, C_6D_6): δ = −0.17 [q, 4H, J = 8.26 Hz, –Mg–*CH*$_2$–CH$_3$], 1.25–1.23 [m, 6H, –Mg–CH$_2$–*CH*$_3$], 1.29 [d, J = 6.72 Hz, 12H, –CH–(CH_3)$_2$], 1.38 [d, J = 7.02 Hz, 12H, –CH–(CH_3)$_2$], 1.63 [s, 6H, –CH_3], 3.29 [spt, J = 6.72 Hz, 4H, –*CH*–(CH_3)$_2$], 3.62 [s, 16H, –*dioxane*], 4.82 [s, 2H, –*H*], 7.20 [s, 6H, *Ar*]. ^{13}C NMR (100 MHz, C_6D_6) δ = −2.75 [–Mg–*CH*$_2$–CH$_3$], 13.73 [–Mg–CH$_2$–*CH*$_3$], 24.35 [–CH_3], 24.74 [–CH–(CH_3)$_2$], 25.16 [–CH–(CH_3)$_2$], 28.67 [–*CH*–(CH_3)$_2$], 67.94 [–*dioxane*], 94.48 [–*CH*], 124.25 [–*m*-CH_{arom}], 125.86 [–*o*-CH_{arom}], 142.8 [–*o*-C_{arom}], 145.65 [–i-C_{arom}], 168.63 [–*CN*], 174.37 [–*CO*]; IR(ATR): $\tilde{\nu}$ = 3055, 2961, 2926, 2864, 2825, 1530, 1456, 1435, 1381, 1366, 1310, 1297, 1256, 1217, 1167, 1120, 1100, 1064, 995, 965, 936, 919, 891, 872, 850, 831, 816, 796, 775, 762, 738, 697, 677 cm^{-1}; elemental analysis calculated (found) $C_{43}H_{68}Mg_2N_2O_5$: C 69.64 (68.17), H 9.24 (9.31), N 3.78 (3.60).

(BODDI)$_2$Mg$_2$. A Schlenk-flask equipped with a stirring bar was charged with **(BODDI)H$_2$** (1 g, 2.17 mmol, 1 equiv.), Mg(HMDS)$_2$ (0.749 g, 2.17 mmol, 1 equiv.) and 5 mL toluene under inert conditions. The solution was stirred at 90 °C for 8 h. A yellow precipitate formed during the reaction which was filtered of and washed with *n*-hexane. The product was obtained as yellow needles (0.667 g, 74% yield). Crystals suitable for X-ray analysis were obtained by cooling a saturated solution in toluene from 90 °C to rt. ^{1}H NMR (250 MHz, C_6D_6): δ = 0.14 [d, J = 6.7 Hz, 6H, –CH(CH_3)$_2$], 1.15 [d, J = 6.8 Hz, 6H, –CH(CH_3)$_2$], 1.33 [d, J = 6.7 Hz, 6H, –CH(CH_3)$_2$], 1.48 [d, J = 7.0 Hz, 6H, –CH(CH_3)$_2$], 1.60 [s, 6H, –CH_3], 2.76 [quin, J = 6.8 Hz, 2H, –*CH*(CH$_3$)$_2$], 3.49 [quin, J = 6.7 Hz, 2H–*CH*(CH$_3$)$_2$], 4.97 [s, 2H, –C*H*], 7.03–6.94 [m, 7H, Ar*H*]. ^{13}C NMR (101 MHz, C_6D_6): δ = 23.39 [–CH(CH_3)$_2$], 24.65 [–CH(CH_3)$_2$], 24.87 [–CH(CH_3)$_2$], 24.97 [–CH_3], 26.42 [–CH(CH_3)$_2$], 28.64 [–*CH*(CH$_3$)$_2$], 29.62 [–*CH*(CH$_3$)$_2$], 95.10 [–*CH*], 123.78 [–CH$_{arom}$], 125.16 [–CH$_{arom}$], 125.70 [–CH$_{arom}$], 141.74 [–C$_{arom}$], 144.33 [–C$_{arom}$], 146.69 [–C$_{arom}$], 171.96 [–CN], 174.99 [–CO]; IR(ATR): $\tilde{\nu}$ = 2960, 2924, 2869, 1655, 1604, 1582, 1524, 1506, 1433, 1381, 1360, 1319, 1269, 1252, 1240, 1210, 1165, 1100, 1051, 965, 924, 850, 796, 760, 702, 680 cm^{-1}; elemental analysis calculated (found) $C_{62}H_{84}N_4Mg_2O_2$: C 77.09 (76.42), H 8.77 (8.77), N 5.80 (5.63).

(BODDI)H(CaHMDS). A Schlenk-flask equipped with a stirring bar was charged with **(BODDI)H$_2$** (0.700 g, 1.52 mmol, 1 equiv.) and 3 mL THF under inert conditions. A solution of Ca(HMDS)$_2$·(thf)$_2$ (0.845 g, 1.67 mmol, 1.1 equiv.) in 4 mL THF was added at 0 °C. The solution was slowly warmed up to room temperature while stirring for 14 h. The product precipitated from the reaction mixture (0.53 g, 53%). ^{1}H NMR (400 MHz, C_6D_6): δ = −0.02–0.05 [m, 18 H, Si–CH_3], 1.18–1.27 [m, 24 H, CH(CH_3)$_2$], 1.47 [m, THF], 1.52 [s, 3 H, –CH_3], 1.69 [s, 3 H, –CH_3], 3.12–3.23 [m, 2 H, *CH*–(CH$_3$)$_2$], 3.40–3.51 [m, 2 H, *CH*–(CH$_3$)$_2$], 3.86 [m, THF], 4.99 [s, 1 H, CH$_3$CN*CH*], 5.01 [s, 1 H, CH$_3$CN*CH*], 7.06–7.17 [m, 6H, *Ar*], 10.22 [s, 1 H, *NH*]. ^{13}C NMR (75 MHz, C_6D_6): δ = 5.76, 20.72, 24.00, 25.04, 25.12, 25.89, 28.25, 28.89, 70.10, 97.72, 98.44, 123.96, 124.50, 125.04, 125.16, 136.15, 141.56, 147.82, 148.14, 153.21, 169.22, 180.52; IR(ATR): 2960, 2868, 1610, 1498, 1461, 1433, 1392, 1333, 1312, 1245, 1236, 1215, 1161, 1100, 1064, 1036, 1006, 993, 954, 913, 876, 828, 820, 809, 792, 764, 755, 744, 714, 697, 682, 658 cm^{-1}; elemental analysis calculated (found) $C_{45}H_{77}CaN_3O_3Si_2$: C 67.19 (66.91); H 9.65 (9.24); N 5.22 (5.26).

(BODDI)$_2$Ca$_2$*THF$_2$. A solution of **(BODDI)H(CaHMDS)** in benzene (0.03 M, 0.55 mL) was heated to 80 °C for 2 h and then all volatiles were removed in vacuum. (7 mg, 74%). ^{1}H NMR (300 MHz, THF-d$_8$): δ [ppm] = 0.48 (d, J = 6.71 Hz, 6 H,

Open Access Article. Published on 09 October 2025. Downloaded on 4/7/2026 7:46:47 PM. This article is licensed under a Creative Commons Attribution 3.0 Unported Licence.

CH(CH_3)$_2$), 0.78 (d, J = 6.71 Hz, 6 H, CH(CH_3)$_2$), 0.98 (br d, J = 6.80 Hz, 12 H, CH(CH_3)$_2$), 1.04–1.11 (THF), 1.26 (d, J = 6.80 Hz, 6 H, CH(CH_3)$_2$), 1.39 (s, 6 H, α-CH_3), 1.47 (br d, J = 6.71 Hz, 6 H, CH(CH_3)$_2$), 1.56 (s, 6 H, α-CH_3), 2.06–2.20 (m, 2 H, C*H*Me$_2$), 2.83–2.95 (m, 2 H, C*H*Me$_2$), 3.04–3.21 (m, 4 H, C*H*Me$_2$), 4.70 (s, 2 H, β-CH), 4.74 (s, 2 H, β-CH), 6.88–7.15 (m, 12 H, ArH). ^{13}C NMR (100 MHz, C_6D_6): δ [ppm] = 23.65, 23.71, 23.92, 24.40, 25.06, 25.08, 25.15, 25.43, 27.87, 27.99, 29.96, 31.98, 95.85, 96.32, 123.50, 123.64, 123.77, 123.90, 124.06, 141.49, 142.09, 142.63, 143.13, 149.73, 150.57, 116.01, 166.04, 175.97. IR(ATR): 2961, 2937, 2870, 1612, 1498, 1461, 1433, 1394, 1314, 1245, 1236, 1215, 1161, 1100, 1066, 1036, 1008, 992, 954, 934, 913, 876, 828, 820, 807, 792, 764, 755, 744, 731, 716, 697, 684, 658 cm^{-1}; elemental analysis calculated (found) $C_{70}H_{100}Ca_2N_4O_4$: C 73.64 (70.15), H 8.83 (8.91), N 4.91 (5.06).

Synthesis of (BODDI)(CaBn)$_2$. A Schlenk-flask equipped with a stirring bar was charged with **(BODDI)H$_2$** (1.0 g, 2.17 mmol, 1 equiv.) and 40 mL toluene under inert conditions. A solution of Ca(Bn)$_2$(thf)$_4$ (2.439 g, 4.78 mmol, 2.2 equiv.) in 8 mL THF was added at −90 °C. The solution was slowly warmed up to room temperature while stirring for 16 h. The volume of the reaction mixture was reduced under vacuum and cooling to 7 °C yielded the product as a crystalline material, which was isolated by filtration (0.55 g, 29%). Crystals suitable for X-ray analysis were obtained by cooling a saturated solution in *n*-hexane (**(BODDI)(CaBn)$_2$_a**) or toluene (**(BODDI)(CaBn)$_2$_b**) from room temperature to 7 °C. ^{1}H NMR (300 MHz, C_6D_6) δ = 1.07 [t, J = 6.4 Hz, 4H, THF], 1.18 [d, J = 6.9 Hz, 24H, –CH–(CH_3)$_2$], 1.73 [s, 6H, –CH_3], 2.13 [s, br, 4H, –Ca–CH_2–Ph], 2.99 [t, J = 6.1 Hz, 4H, THF], 3.27 [quin, J = 6.8 Hz, 4H, –*CH*–(CH$_3$)$_2$], 5.17 [s, 2H, –*H*], 5.91 [t, J = 6.8 Hz, 2H, –*p*-$CH_{arom,\ CaBn}$], 6.66–6.54 [m, 8H, –*o*,*m*-$CH_{arom,\ CaBn}$], 7.12–7.00 [m, 6H, Ar–*H*]; ^{13}C NMR (75 MHz, C_6D_6) δ = 24.61 [–CH–(CH_3)$_2$], 25.08 [–CH_3], 25.15 [–CH–(CH_3)$_2$], 25.42 [THF], 28.61 [–*CH*–(CH$_3$)$_2$], 45.84 [–Ca–CH_2–Ph], 69.05 [THF], 95.97 [–*CH*], 110.45 [–$CH_{arom,\ CaBn}$], 120.41 [–$CH_{arom,\ CaBn}$], 124.05 [–*m*-CH_{arom}], 124.21, [–*p*-CH_{arom}] 131.01 [–$CH_{arom,\ CaBn}$], 142.68 [–i-$C_{arom,\ CaBn}$], 148.51 [–*o*-C_{arom}], 157.43 [–i-C_{arom}], 165.11 [–*CN*], 176.96 [–*CO*]; IR(ATR): 2958, 1577, 1519, 1472, 1457, 1429, 1377, 1327, 1310, 1295, 1271, 1252, 1236, 1213, 1185, 1161, 1096, 1068, 1053, 1023, 988, 932, 911, 891, 874, 852, 837, 792, 764, 755, 738, 727, 703, 688, 671 cm^{-1}; elemental analysis calculated (found) $C_{53}H_{70}Ca_2N_2O_3$: C 73.74 (71.00); H 8.17 (7.95); N 3.24 (3.31).

(BODDI)H(ZnHMDS). A Schlenk-flask equipped with a stirring bar was charged with **(BODDI)H$_2$** (0.335 g, 0.727 mmol, 1 equiv.) and 4.5 mL toluene under inert conditions. Zn(HMDS)$_2$ (0.30 mL, 0.74 mmol, 1 equiv.) was added dropwise at 0 °C. The solution was warmed up to room temperature, while stirring overnight. The solvent was removed under reduced pressure and the residue was dissolved in *n*-hexane. The product was obtained by crystallization at −80 °C (0.273 g, 54%). ^{1}H NMR (300 MHz, C_6D_6): δ = 0.10–0.15 [s, 18 H, Si–CH_3], 1.10 [dd, J = 10.71, 6.89 Hz, 12 H, CH–(CH_3)$_2$], 1.28 [dd, J = 11.22, 6.85 Hz, 12 H, –CH–(CH_3)$_2$], 1.46 [s, 3 H, –CH_3], 1.59 [s, 3 H, –CH_3], 3.14–3.27 [m, 2 H, C*H*–(CH$_3$)$_2$], 3.27–3.39 [C*H*–(CH$_3$)$_2$], 4.99 [s, 1 H, –C*H*], 5.10 [s, 1 H, –C*H*], 7.02–7.14 [m, 6 H, *Ar*], 10.75 [s, 1 H, *NH*]. ^{13}C NMR (75 MHz, C_6D_6): δ = 5.78, 20.38, 23.15, 24.30, 24.70, 28.77, 29.09, 96.71, 97.22, 124.15, 124.64, 128.24, 128.56, 134.90, 143.02, 144.19, 147.51, 158.87, 171.44, 185.09; IR(ATR): 2961, 2870, 1616, 1506, 1467, 1437, 1388, 1320, 1275, 1254, 1245, 1213, 1170, 1100, 1053, 982, 962, 928, 880, 863, 831, 818, 798, 762, 755, 747, 710, 690, 669 cm^{-1}; elemental analysis calculated (found) $C_{41}H_{69}N_3O_2Si_2Zn$: C 65.00 (64.93), H 9.18 (8.82), N 5.55 (6.02).

(BODDI)H(ZnEt). A Schlenk-flask equipped with a stirring bar was charged with **(BODDI)H$_2$** (2 g, 4.34 mmol, 1 equiv.) and 40 mL toluene under inert conditions. A solution of $ZnEt_2$ 1 M in *n*-hexanes (9 mL, 9.55 mmol, 2.2 equiv.) was added and the solution was stirred at room temperature overnight. All volatiles were removed under reduced pressure and the residue was dissolved in 21 mL hot *n*-hexane. The solution was filtered and the product crystallized from the solution at rt. Crystallization proceeded further by cooling to −30 °C. Yellow crystals were obtained (1.46 g, 61%). ^{1}H NMR (400 MHz, C_6D_6): δ = 0.61 [q, J = 8.2 Hz, 2H, –Zn–CH_2–CH_3], 1.17–1.00 [m, 24H, –CH–(CH_3)$_2$], 1.35 [t, J = 8.2 Hz, 3H, –Zn–CH_2–CH_3], 1.48 [s, 3H, –CH_3], 1.56 [s, 3H, –CH_3], 3.06 [quin, J = 6.9 Hz, 2H, –*CH*–(CH$_3$)$_2$], 3.34 [quin, J = 6.9 Hz, 2H, –*CH*–(CH$_3$)$_2$], 5.12 [s, 1H, –*CH*], 5.24 [s, 1H, –*CH*], 7.14–7.03 [m, 6H, –Ar–*H*], 10.94 [s, 1H, –*NH*]; ^{13}C NMR (100 MHz, C_6D_6): δ = −1.57 [–Zn–CH_2–CH_3], 12.93 [–Zn–CH_2–CH_3], 20.35 [–CH_3], 22.77 [–CH–(CH_3)$_2$], 23.56 [–CH–(CH_3)$_2$], 23.69 [–CH_3], 24.75 [–CH–(CH_3)$_2$], 25.39 [–CH–(CH_3)$_2$], 28.64 [–*CH*–(CH$_3$)$_2$], 29.18 [–*CH*–(CH$_3$)$_2$], 97.03 [–*CH*], 97.30 [–*CH*], 124.11 [–*m*-C_{arom}], 124.16 [–*m*-C_{arom}], 126.48 [–*p*-C_{arom}], 135.49 [–i-C_{arom}], 142.68 [–*o*-C_{arom}], 144.72 [–i-C_{arom}], 147.82 [–*o*-C_{arom}], 157.80 [–*CN*], 169.85 [–*CN*], 184.57 [–*CO*]; IR(ATR): $\tilde{\nu}$ = 2960, 2922, 2896, 2866, 2855, 1616, 1601, 1528, 1504, 1463, 1439, 1387, 1368, 1316, 1265, 1254, 1224, 1210, 1170, 1144, 1098, 1049, 1008, 965, 934, 921, 898, 882, 861, 833, 798, 762, 753, 736, 721, 708, 686 cm^{-1}; elemental analysis calculated (found) $C_{33}H_{48}N_2OZn$: C 71.53 (71.69), H 8.73 (8.79), N 5.06 (5.06).

(BODDI)(ZnHMDS)$_2$. A Schlenk-flask equipped with a stirring bar was charged with **(BODDI)H$_2$** (2.7 g, 5.86 mmol, 1 equiv.) and 50 mL toluene under inert conditions. Zn(HMDS)$_2$ (7.1 mL, 17.58 mmol, 3 equiv.) was added and the solution was stirred at 75 °C for 13 days. The solvent was removed under reduced pressure and the residue was recrystallized from hot *n*-hexane. The product was obtained as yellow crystals (3.97 g 74%). Crystals suitable for X-ray analysis were obtained by crystallization from toluene at −30 °C. ^{1}H NMR (400 MHz, C_6D_6): δ = 0.20 [s, br, 36H, –Si(CH_3)$_3$], 1.18 [d, J = 6.7 Hz, 12H, –CH–(CH_3)$_2$], 1.41 [d, J = 6.8 Hz, 12H, –CH–(CH_3)$_2$], 1.53 [s, 6H, –CH_3], 3.33 [s, br, 4H –*CH*–(CH$_3$)$_2$], 4.77 [s, 2H, –*H*], 7.14 [s, 6H]. ^{13}C NMR (100 MHz, C_6D_6): δ = 6.03 [–Si(CH_3)$_3$], 24.38 [–CH–(CH_3)$_2$], 24.64 [–CH_3], 29.05 [–*CH*–(CH$_3$)$_2$], 96.43 [–*CH*], 124.71 [–*m*-CH_{arom}], 127.20 [–*p*-CH_{arom}], 143.46 [–*o*-C_{arom}], 144.15 [–i-C_{arom}], 170.61 [–*CN*], 178.30 [–*CO*]; ^{29}Si NMR (80 MHz, C_6D_6): δ = −2.32; IR(ATR): $\tilde{\nu}$ = 3060, 2960, 2870, 1536, 1461, 1433, 1375, 1359, 1336, 1316, 1278, 1269, 1243, 1217, 1176, 1111, 1098, 990, 932, 876, 861, 842, 826, 816, 798, 772,

 This journal is © The Royal Society of Chemistry 2025

Open Access Article. Published on 09 October 2025. Downloaded on 4/7/2026 7:46:47 PM. This article is licensed under a Creative Commons Attribution 3.0 Unported Licence.

764, 755, 695, 669 cm^{-1}; elemental analysis calculated (found) $C_{43}H_{78}N_4OSi_4Zn_2$: C 56.74 (57.74), H 8.64 (8.72), N 6.16 (6.17).

(BODDI)(ZnEt)$_2$. Following a literature procedure, a Schlenk-flask equipped with a stirring bar was charged with **(BODDI)H$_2$** (2 g, 4.34 mmol, 1 equiv.) and 40 mL toluene under inert conditions. A solution of $ZnEt_2$ 1 M in *n*-hexanes (9.6 mL, 9.55 mmol, 2.2 equiv.) was added and the solution was stirred at 75 °C for 22 h. The solvent was removed under reduced pressure. The residue was dissolved in hot *n*-hexane and the product crystallized at room temperature. The product was obtained as yellow needles (2.19 g, 78% yield). ^{1}H NMR (400 MHz, C_6D_6): δ = 0.68 [q, J = 8.18 Hz, 4H, –Zn–CH_2–CH_3], 1.11 [d, J = 6.72 Hz, 12H, –CH–(CH_3)$_2$], 1.14 [d, J = 6.72 Hz, 12H, –CH–(CH_3)$_2$], 1.19 [t, J = 8.18 Hz, 6H, –Zn–CH_2–CH_3], 1.56 [s, 6H, –CH_3], 3.18 [spt, J = 6.87 Hz, 4H, –CH–(CH_3)$_2$], 5.05 [s, 2H, –CH], 7.12–7.04 [m, 6H, Ar–H]. ^{13}C NMR (100 MHz, C_6D_6): δ = 0.72 [–Zn–CH_2–CH_3], 12.64 [–Zn–CH_2–CH_3], 23.73 [–CH_3], 24.80 [–CH–(CH_3)$_2$], 28.70 [–CH–(CH_3)$_2$], 96.13 [–CH], 124.24 [–*m*-CH_{arom}], 126.65 [–*p*-CH_{arom}], 143.19 [–*o*-C_{arom}], 144.40 [–i-C_{arom}], 167.56 [–CN], 177.83 [–CO]; IR(ATR): $\tilde{\nu}$ = 3055, 2958, 2863, 1534, 1456, 1435, 1375, 1362, 1316, 1275, 1252, 1215, 1174, 1146, 1100, 1055, 1042, 993, 986, 960, 945, 932, 895, 885, 861, 796, 781, 760, 742, 721, 699, 671 cm^{-1}; elemental analysis calculated (found) $C_{35}H_{52}N_2OZn_2$: C 64.92 (65.70), H 8.09 (8.18), N 4.33 (4.32).

Polymerization of L-lactide

A 0.4 mol L^{-1} solution of L-lactide (used as received without further purification or drying or recrystallized and sublimed twice) in dry THF was treated with the related complex at 30 °C ± 1.9 °C at the catalyst : monomer ratios stated in Tables 1 and 2. The reaction progress was monitored using *in situ* IR spectroscopy. Please note that due to the fast reactions and the time increments of the spectrometer not enough data points could be obtained for a detailed investigation of reactions rates and orders. Thus, the time until 60% conversion was measured and a part of the reaction mixture was quenched by adding a 1 M solution of hydrochloric acid in methanol and the formed polymer was precipitated using methanol. In addition, the remaining reaction mixture was quenched at the end of the reaction (t_{total}) and analyzed as well. The obtained material was characterized with respect to its dispersity $Đ$ and the number average molecular weight M_n by size-exclusion chromatography (SEC), the values are uncorrected.

X-ray crystallography

The intensity data for the compound **(BODDI)H(MgHMDS)** were collected on a Siemens SMART three axis diffractometer with APEX II area detector while all other single crystal X-ray diffraction data were recorded Nonius KappaCCD diffractometer using monochromated Mo-K_α radiation. Data were corrected for Lorentz and polarization effects; absorption was taken into account on a semi-empirical basis using multiple-scans.[34] The structures were solved by direct methods (SHELXT)[35] and refined by full-matrix least squares techniques against F_o^2 (SHELXL-2018).[36] The hydrogen atoms bonded to the amine group N_2 of the compounds **(BODDI)H(MgHMDS)**, **(BODDI)H(CaHMDS)**, and **(BODDI)H(ZnHMDS)** as well as those bound to C38 and C45 of **(BODDI)(CaBn)2_a** and **(BODDI)(CaBn)2_b** were located by difference Fourier synthesis and refined isotropically. All other hydrogen atoms were included at calculated positions with fixed thermal parameters. All non-hydrogen atoms were refined anisotropically.[36] The crystal of **(BODDI)H(CaHMDS)** was a non-merohedral twin. The twin law was determined by PLATON[37] to (1.000 0.034 0.066) (0.000–1.000 0.000) (0.000 0.000–1.000). The contribution of the main component were refined to 0.783(2). Additionally, the crystals of **(BODDI)H(CaHMDS)** and **(BODDI)$_2$Mg$_2$** contain large voids, filled with disordered solvent molecules. The size of the voids are 967, and 968 Å^3 per unit cell, respectively. Their contribution to the structure factors was secured by back-Fourier transformation using the SQUEEZE routine of the program PLATON[37] resulting in 354, and 242 electrons per unit cell, respectively. Furthermore, the crystals of **(BODDI)(MgEt)$_2$** were extremely thin and of low quality, resulting in a substandard data set; however, the data are sufficient to show connectivity and geometry despite the high final R value. We hence only present the conformation of the molecule and the crystallographic data but will not deposit the data in the Cambridge Crystallographic Data Centre.

Table 2 Catalytic data for the ROP of L-lactide. Conversions were deduced from *in situ* IR spectroscopy. Reaction conditions: room temperature, THF, monomer concentration 0.4 mol L^{-1}, SEC data was obtained by calibration with PMMA standards in $CHCl_3$/i-PrOH/NEt_3 94 : 2 : 4

Entry	Cat	Cat : mon ratio	$t_{60\%}$ [a] [min]	$Đ$ SEC (M_w/M_n)	M_n SEC (g mol^{-1})	t_{total} [b] [min]	$Đ$ SEC (M_w/M_n)	M_n SEC (g mol^{-1})
12	**(BODDI)Li$_2$**	1 : 200	0.78	1.50	2.79×10^4	10 (96%)	1.59	3.74×10^4
13	**(BODDI)(MgHMDS)$_2$**	1 : 200	1.02	1.60	5.50×10^4	1.94 (89%)	1.57	5.55×10^4
14	**(BODDI)(MgEt)$_2$**	1 : 200	0.10	1.47	2.74×10^4	2.89 (94%)	1.44	3.00×10^4
15	**(BODDI)(MgH)$_2$**	1 : 200	—	—	—	60 (42%)	1.39	3.08×10^4
16	**(BODDI)$_2$Mg$_2$**	1 : 200	9.17	1.40	3.99×10^4	88 (90%)	1.47	5.30×10^4
17	**(BODDI)(CaBn)$_2$**	1 : 200	89.44	—	—	—	—	—
18	**(BODDI)$_2$Ca$_2$**	1 : 200	—	—	—	80 (58%)	1.43	2.67×10^4
19	**(BODDI)(ZnHMDS)$_2$**	1 : 200	133.37	1.82	3.83×10^4	600 (99%)	1.43	6.14×10^4
20	**(BODDI)(ZnEt)$_2$**	1 : 200	—	—	—	—	—	—

[a] The reaction progress was monitored using *in situ* IR spectroscopy. $t_{60\%}$ refers to the reaction time required to reach 60% conversion. [b] Time at which the reaction was quenched, *i.e.*, when no further progress was observed.

Open Access Article. Published on 09 October 2025. Downloaded on 4/7/2026 7:46:47 PM.
This article is licensed under a Creative Commons Attribution 3.0 Unported Licence.

Table 3 Catalytic data for the ROP of L-lactide for mechanistic studies. Conversions were deduced from *in situ* IR spectroscopy. Reaction conditions: room temperature, THF, monomer concentration 0.4 mol L^{-1}, SEC data was obtained by calibration with PMMA standards in $CHCl_3$/i-PrOH/NEt_3 94 : 2 : 4. The data also show the reproducibility of the results

Entry	Cat	Cat : mon ratio	I : mon ratio	$t_{60\%}$[a] [min]	$Đ$[b] SEC (M_w/M_n)	M_n[b] SEC (g mol^{-1})	t_{total}[c] [min]	$Đ$ SEC (M_w/M_n)	M_n SEC (g mol^{-1})	Quality of L-lactide
21		1 : 200	—	1 : 50	2.15	5.1×10^4	4 : 30 (89%)	2.15	5.9×10^4	Used as delivered
22	**(BODDI)(MgHMDS)$_2$**	1 : 200	—	1 : 35	—	—	4 : 10 (92%)	—	—	Purified (recrystallized and sublimed twice)
23		1 : 200	1 : 200	1 : 00	1.72	3.1×10^4	7 : 50 (79%)	1.95	3.6×10^4	
24		1 : 200	—	10 : 09	1.64	6.5×10^4	32 : 00 (90%)	1.69	1.9×10^4	Used as delivered
25	**(BODDI)$_2$Mg$_2$**	1 : 200	—	4 : 00	1.63	3.5×10^4	11 : 20 (97%)	1.78	7.7×10^4	Purified (recrystallized and sublimed twice)
26		1 : 200	1 : 200	3 : 10	1.40	1.9×10^4	9 : 50 (82%)	1.71	4.0×10^4	

[a] The reaction progress was monitored using *in situ* IR spectroscopy. $t_{60\%}$ refers to the reaction time required to reach 60% conversion. [b] Conversion: entry 21: 20–30%; entry 22: 30–40%; entry 23: 30–40%; entry 24: 25%; entry 25: 25%; entry 26: 20%. [c] Time at which the reaction was quenched, *i.e.*, when no further progress was observed.

Crystallographic data as well as structure solution and refinement details are summarized in Table S1 of the SI. Olex2 was used for structure representations.[38]

Crystallographic data (excluding structure factors) has been deposited with the Cambridge Crystallographic Data Centre as supplementary publication CCDC 2247495 for **(BODDI)H(MgHMDS)**, 2247496 for **(BODDI)(MgHMDS)$_2$**, 2247497 for **(BODDI)$_2$Mg$_2$**, 2247498 for **(BODDI)H(CaHMDS)**, 2247499 for **(BODDI)$_2$Ca$_2$**, 2247500 for **(BODDI)(CaBn)$_2$_a**, 2251441 for **(BODDI)(CaBn)$_2$_b**, 2247501 for **(BODDI)H(ZnHMDS)**, and 2247502 for **(BODDI)(ZnHMDS)$_2$**.

Mechanistic studies

A 0.4 mol L^{-1} solution of L-lactide (used as purchased and with further purification or recrystallized and sublimed twice) in dry THF was treated with the selected catalysts (**(BODDI)(MgHMDS)$_2$** and **(BODDI)$_2$Mg$_2$**) at the catalyst : monomer and initiator : monomer ratios stated in Table 3. The reaction progress was monitored using *in situ* IR spectroscopy. The time until 20–40% conversion was measured, and a part of the reaction mixture was quenched by adding a 1 M solution of hydrochloric acid in methanol and the formed polymer was precipitated using methanol. In addition, the remaining reaction mixture was quenched at the end of the reaction (t_{total}) and analyzed as well. The obtained material was characterized with respect to its polydispersity $Đ$ and the number average molecular weight M_n by size-exclusion chromatography (SEC) and MALDI-TOF and end-group analysis *via* ^{1}H NMR-spectroscopy, the values are uncorrected.

End-group analysis *via* ^{1}H NMR-spectroscopy

The proton NMR spectra were recorded at 500 MHz on a Bruker NEO spectrometer. Chemical shifts (δ in ppm) were referenced to the residual solvent signal, $CHCl_3$ in $CDCl_3$ at δ = 7.26. All NMR spectra were processed uniformly using TopSpin 4.4.1 (Bruker). Phase correction and baseline correction were performed within the software. The integrals of the methine group of the end group, the hydroxy group, and the repeating unit were determined. These integrals were directly proportional to the molar concentration of the respective molecule. Thus, the average number of repeating units within the polymer chains (number average degree of polymerization, DP_n) were determined.

MALDI-TOF mass spectrometry

The matrix-assisted laser desorption/ionization spectra were acquired with a BRUKER autoflex MALDI-TOF instrument in the positive ion and linear modes. The laser of this instrument is a smartbeam-II with a wavelength of 355 nm. The software for measurement and evaluation of the spectra is flexControl 3.4 and flexAnalysis 3.4 and Polymerix. The spectra were calibrated externally using poly(methyl methacrylate) (PMMA) as a standard.

The samples were prepared on a standard sample plate (Bruker "MTP 384 target plate polished steel BC"). Sample spot preparation was as follows 10 μL of 20 mg mL^{-1} *trans*2-[3-(4-*tert*-butylphenyl)-2-methyl-2-propenylidene] malononitrile (DCTB) matrix chloroform solution, 0.5 μL sodium trifluoroacetate (NaTFA, 0.1 M in THF) solution, and 1.5 μL polymer sample (2 mg mL^{-1} in chloroform) were mixed. Then 1 μL of this matrix/salt/polymer solution was spotted onto a MALDI sample plate and air dried before analysis.

Conflicts of interest

There are no conflicts to declare.

Data availability

The data supporting this article have been included as part of the supplementary information (SI). Supplementary information: for additional figures, crystallographic data, NMR and IR spectra, details on the end-group analysis as well as a proposed mechanism. See DOI: **https://doi.org/10.1039/d5dt01934f**.

This journal is © The Royal Society of Chemistry 2025

Open Access Article. Published on 09 October 2025. Downloaded on 4/7/2026 7:46:47 PM. This article is licensed under a Creative Commons Attribution 3.0 Unported Licence.

CCDC 2247495 **(BODDI)H(MgHMDS)**, 2247496 **(BODDI)(MgHMDS)$_2$**, 2247497 **(BODDI)$_2$Mg$_2$**, 2247498 **(BODDI)H(CaHMDS)**, 2247499 **(BODDI)$_2$Ca$_2$**, 2247500 **(BODDI)(CaBn)$_2$_a**, 2247501 **(BODDI)H(ZnHMDS)**, 2247502 **(BODDI)(ZnHMDS)$_2$** and 2251441 **(BODDI)(CaBn)$_2$_b** contain the supplementary crystallographic data for this paper.[39a–i]

Acknowledgements

The work is dedicated to Wolfgang Weigand on the occasion of his 65th birthday. The project was financially supported by the Deutsche Forschungsgemeinschaft (DFG, KR4782/3-1), the Friedrich Schiller University Jena, the University Duisburg-Essen, and the Chemnitz University of Technology. We are thankful to Grit Festag at FSU Jena for conducting the SEC measurements and to the Deutsche Forschungsgemeinschaft for supporting the research infrastructure (INST 270/319-1 FUGG, project 437101278; INST 270/347-1 FUGG, project 446537989; INST 270/363-1 FUGG, project 530103110).

References

1 (*a*) Y. Zhu, C. Romain and C. K. Williams, *Nature*, 2016, **540**, 354; (*b*) D. K. Schneiderman and M. A. Hillmyer, *Macromolecules*, 2017, **50**, 3733; (*c*) *European Bioplastics*, nova-Institute, 2021, **https://www.european-bioplastics.org/tag/nova-institut/**.

2 T. P. Haider, C. Völker, J. Kramm, K. Landfester and F. R. Wurm, *Angew. Chem., Int. Ed.*, 2019, **58**, 50.

3 (*a*) E. Castro-Aguirre, F. Iñiguez-Franco, H. Samsudin, X. Fang and R. Auras, *Adv. Drug Delivery Rev.*, 2016, **107**, 333; (*b*) M. S. Singhvi, S. S. Zinjarde and D. V. Gokhale, *J. Appl. Microbiol.*, 2019, **127**, 1612.

4 E. Fazekas, P. A. Lowy, M. Abdul Rahman, A. Lykkeberg, Y. Zhou, R. Chambenahalli and J. A. Garden, *Chem. Soc. Rev.*, 2022, **51**, 8793.

5 (*a*) *Cooperative Catalysis: Designing Efficient Catalysts for Synthesis*, ed. R. Peters, Wiley, 2015; (*b*) P. Kalck, *Homo- and Heterobimetallic Complexes in Catalysis*, Springer International Publishing, Cham, 2016, vol. 59; (*c*) J. M. Gil-Negrete and E. Hevia, *Chem. Sci.*, 2021, **23**, 1982–1992.

6 (*a*) I. Yu, A. Acosta-Ramírez and P. Mehrkhodavandi, *J. Am. Chem. Soc.*, 2012, **134**, 12758; (*b*) M. Normand, T. Roisnel, J.-F. Carpentier and E. Kirillov, *Chem. Commun.*, 2013, **49**, 11692; (*c*) W.-L. Kong and Z.-X. Wang, *Dalton Trans.*, 2014, **43**, 9126; (*d*) H.-C. Huang, B. Wang, Y.-P. Zhang and Y.-S. Li, *Polym. Chem.*, 2016, **7**, 5819; (*e*) G. Trott, J. A. Garden and C. K. Williams, *Chem. Sci.*, 2019, **10**, 4618; (*f*) A. B. Kremer and P. Mehrkhodavandi, *Coord. Chem. Rev.*, 2019, **380**, 35; (*g*) A. C. Deacy, A. F. R. Kilpatrick, A. Regoutz and C. K. Williams, *Nat. Chem.*, 2020, **12**, 372; (*h*) W. Gruszka and J. A. Garden, *Nat. Commun.*, 2021, **12**, 3252; (*i*) A. J. Gaston, Z. Greindl, C. A. Morrison and J. A. Garden, *Inorg. Chem.*, 2021, **60**, 2294; (*j*) F. Fiorentini, W. T. Diment, A. C. Deacy, R. W. F. Kerr, S. Faulkner and C. K. Williams, *Nat. Commun.*, 2023, **14**, 4783; (*k*) L.-J. Wu, W. Lee, P. Kumar Ganta, Y.-L. Chang, Y.-C. Chang and H.-Y. Chen, *Coord. Chem. Rev.*, 2023, **475**, 214847; (*l*) M. Abdul Rahman, T. J. Neal and J. A. Garden, *Chem. Commun.*, 2024, **60**, 5530; (*m*) P. A. Lowy, M. Abdul Rahman, G. S. Nichol, C. A. Morrison and J. A. Garden, *ChemCatChem*, 2024, **16**, e202301338; (*n*) U. Yolsal, P. J. Shaw, P. A. Lowy, R. Chambenahalli and J. A. Garden, *ACS Catal.*, 2024, **14**, 1050; (*o*) F. Fiorentini, K. H. S. Eisenhardt, A. C. Deacy and C. K. Williams, *J. Am. Chem. Soc.*, 2024, **146**, 23517; (*p*) E. J. K. Shellard, W. T. Diment, D. A. Resendiz-Lara, F. Fiorentini, G. L. Gregory and C. K. Williams, *ACS Catal.*, 2024, **14**, 1363; (*q*) F. Butler, F. Fiorentini, K. H. S. Eisenhardt and C. K. Williams, *Angew. Chem., Int. Ed.*, 2025, **64**, e202422497.

7 R. Kretschmer, *Chem. – Eur. J.*, 2020, **26**, 2099–2119.

8 (*a*) D. F.-J. Piesik, S. Range and S. Harder, *Organometallics*, 2008, **27**, 6178; (*b*) M. Köhler, P. Rinke, K. Fiederling, H. Görls, N. Ueberschaar, F. H. Schacher and R. Kretschmer, *Macromol. Chem. Phys.*, 2021, **222**, 2100187; (*c*) A. Rösch, F. Seifert, V. Vass, H. Görls and R. Kretschmer, *New J. Chem.*, 2021, **18**, 972–981.

9 (*a*) S. Iguchi and A. Inoue, *Chem. Pharm. Bull.*, 1963, **11**, 390; (*b*) M. Himmelsbach, R. L. Lintvedt, J. K. Zehetmair, M. Nanny and M. J. Heeg, *J. Am. Chem. Soc.*, 1987, **109**, 8003.

10 (*a*) S. D. Allen, D. R. Moore, E. B. Lobkovsky and G. W. Coates, *J. Organomet. Chem.*, 2003, **683**, 137; (*b*) S. Li, M. Wang, B. Liu, L. Li, J. Cheng, C. Wu, D. Liu, J. Liu and D. Cui, *Chem. – Eur. J.*, 2014, **20**, 15493; (*c*) H.-C. Chiu, A. J. Pearce, P. L. Dunn, C. J. Cramer and I. A. Tonks, *Organometallics*, 2016, **35**, 2076; (*d*) F. Yan, S. Li, L. Li, W. Zhang, D. Cui, M. Wang and Y. Dou, *Eur. J. Inorg. Chem.*, 2019, **2019**, 2277; (*e*) F. L. Portwich, Y. Carstensen, A. Dasgupta, S. Kupfer, R. Wyrwa, H. Görls, C. Eggeling, B. Dietzek, S. Gräfe, M. Wächtler and R. Kretschmer, *Angew. Chem., Int. Ed.*, 2022, **61**, e202117499.

11 (*a*) R. E. Mulvey, *Chem. Soc. Rev.*, 1991, **20**, 167; (*b*) E. Weiss, *Angew. Chem., Int. Ed. Engl.*, 1993, **32**, 1501; (*c*) A. Downard and T. Chivers, *Eur. J. Inorg. Chem.*, 2001, **2001**, 2193.

12 M. Stender, R. J. Wright, B. E. Eichler, J. Prust, M. M. Olmstead, H. W. Roesky and P. P. Power, *J. Chem. Soc., Dalton Trans.*, 2001, 3465.

13 W.-Y. Lee, H.-H. Hsieh, C.-C. Hsieh, H. M. Lee, G.-H. Lee, J.-H. Huang, T.-C. Wu and S.-H. Chuang, *J. Organomet. Chem.*, 2007, **692**, 1131.

14 (*a*) A. P. Dove, V. C. Gibson, P. Hormnirun, E. L. Marshall, J. A. Segal, A. J. P. White and D. J. Williams, *Dalton Trans.*, 2003, **102**, 3088; (*b*) P. Rinke, H. Görls and R. Kretschmer, *Inorg. Chem.*, 2021, **60**, 5310.

15 T. X. Gentner, B. Rösch, K. Thum, J. Langer, G. Ballmann, J. Pahl, W. A. Donaubauer, F. Hampel and S. Harder, *Organometallics*, 2019, **38**, 2485.

Open Access Article. Published on 09 October 2025. Downloaded on 4/7/2026 7:46:47 PM. This article is licensed under a Creative Commons Attribution 3.0 Unported Licence.

16 S. Krieck, P. Schüler, J. Peschel and M. Westerhausen, *Synthesis*, 2019, 1115.
17 A. M. Johns, S. C. Chmely and T. P. Hanusa, *Inorg. Chem.*, 2009, **48**, 1380.
18 S.-M. Ho, C.-S. Hsiao, A. Datta, C.-H. Hung, L.-C. Chang, T.-Y. Lee and J.-H. Huang, *Inorg. Chem.*, 2009, **48**, 8004.
19 M. H. Chisholm, J. Gallucci and K. Phomphrai, *Chem. Commun.*, 2003, 48.
20 P. Rinke, H. Görls and R. Kretschmer, *Isr. J. Chem.*, 2023, **71**, 171.
21 F. Seifert, H. Görls, S. Kupfer and R. Kretschmer, *Chem. Commun.*, 2023, 7627–7630.
22 B. M. Chamberlain, M. Cheng, D. R. Moore, T. M. Ovitt, E. B. Lobkovsky and G. W. Coates, *J. Am. Chem. Soc.*, 2001, **123**, 3229.
23 L.-F. Hsueh, N.-T. Chuang, C.-Y. Lee, A. Datta, J.-H. Huang and T.-Y. Lee, *Eur. J. Inorg. Chem.*, 2011, **2011**, 5530.
24 J. M. Pérez, C. Ruiz and I. Fernández, *J. Chem. Educ.*, 2022, **99**, 1000.
25 C. R. Rtínez, J. M. Pérez, F. M. Arrabal-Campos, M. Batuecas, M. A. Ortuño and I. Fernández, *Polym. Chem.*, 2021, **12**, 4083.
26 J. Gao, W. Zhang, X. Wang, R. Wang, M. Han, F. Cao and X. Hao, *Catalysts*, 2023, **13**, 770.
27 (*a*) J. Meimoun, A. Favrelle-Huret, M. Bria, N. Merle, G. Stoclet, J. de Winter, R. Mincheva, J.-M. Raquez and P. Zinck, *Polym. Degrad. Stab.*, 2020, **181**, 109188; (*b*) J. Meimoun, A. Favrelle-Huret, J. de Winter and P. Zinck, *Macromol*, 2022, **2**, 236.
28 E. Glöckler, S. Ghosh, C. Wölper, D. Coban, A. H. Gröschel and S. Schulz, *Polyhedron*, 2022, **222**, 115918.
29 (*a*) O. Dechy-Cabaret, B. Martin-Vaca and D. Bourissou, *Chem. Rev.*, 2004, **104**, 6147; (*b*) A. Bhaw-Luximon, D. Jhurry, N. Spassky, S. Pensec and J. Belleney, *Polymer*, 2001, **42**, 9651.
30 L. A. Freeman, J. E. Walley, D. A. Dickie and R. J. Gilliard, *Dalton Trans.*, 2019, **48**, 17174.
31 M. Westerhausen, *Inorg. Chem.*, 1991, **30**, 96.
32 R. Fischer, D. Walther, P. Gebhardt and H. Görls, *Organometallics*, 2000, **19**, 2532.
33 D. Rivillo, H. Gulyás, J. Benet-Buchholz, E. C. Escudero-Adán, Z. Freixa and P. W. N. M. van Leeuwen, *Angew. Chem., Int. Ed.*, 2007, **46**, 7247.
34 (*a*) *COLLECT, Data Collection Software*, Nonius B.V., Delft, The Netherlands, 1998; (*b*) Z. Otwinowski and W. Minor, in *Methods in Enzymology: Macromolecular Crystallography Part A*, ed. C. W. Carter Jr., Academic Press, 1997, vol. 276, pp. 307–326; (*c*) *SADABS 2.10*, Bruker-AXS inc., Madison, WI, U. S.A., 2002.
35 G. M. Sheldrick, *Acta Crystallogr., Sect. A: Found. Adv.*, 2015, **71**, 3.
36 G. M. Sheldrick, *Acta Crystallogr., Sect. C: Struct. Chem.*, 2015, **71**, 3.
37 A. L. Spek, *Acta Crystallogr., Sect. C: Struct. Chem.*, 2015, **71**, 9.
38 O. V. Dolomanov, L. J. Bourhis, R. J. Gildea, J. A. K. Howard and H. Puschmann, *J. Appl. Crystallogr.*, 2009, **42**, 339.
39 (*a*) CCDC 2247495: Experimental Crystal Structure Determination, 2025, DOI: **10.5517/ccdc.csd.cc2ffpvf**; (*b*) CCDC 2247496: Experimental Crystal Structure Determination, 2025, DOI: **10.5517/ccdc.csd.cc2ffpwg**; (*c*) CCDC 2247497: Experimental Crystal Structure Determination, 2025, DOI: **10.5517/ccdc.csd.cc2ffpxh**; (*d*) CCDC 2247498: Experimental Crystal Structure Determination, 2025, DOI: **10.5517/ccdc.csd.cc2ffpyj**; (*e*) CCDC 2247499: Experimental Crystal Structure Determination, 2025, DOI: **10.5517/ccdc.csd.cc2ffpzk**; (*f*) CCDC 2247500: Experimental Crystal Structure Determination, 2025, DOI: **10.5517/ccdc.csd.cc2ffq0m**; (*g*) CCDC 2247501: Experimental Crystal Structure Determination, 2025, DOI: **10.5517/ccdc.csd.cc2ffq1n**; (*h*) CCDC 2247502: Experimental Crystal Structure Determination, 2025, DOI: **10.5517/ccdc.csd.cc2ffq2p**; (*i*) CCDC 2251441: Experimental Crystal Structure Determination, 2025, DOI: **10.5517/ccdc.csd.cc2fkt4z**.

This journal is © The Royal Society of Chemistry 2025